Dick, H.J.B., Natland, J.H., Miller, D.J., et al., 1999
Proceedings of the Ocean Drilling Program, Initial Reports Volume 176

1. Leg 176 Summary[1]

Shipboard Scientific Party[2]

SITE ABSTRACT

Hole 735B

Latitude: 32.723° (32°43.392′S)
Longitude: 57.266° (57°15.960′E)
Start hole: 1345 hr, 24 October 1997
End hole: 1900 hr, 1 December 1997
Time on hole: 917.3 hr (38 days, 5 hr, 15 min; 38.2 days)
Seafloor (drill-pipe measurement from rig floor, mbrf): 731.0
Total depth (drill-pipe measurement from sea level, m): 720.1
Distance between rig floor and sea level (m): 10.9
Total depth (from rig floor, mbrf): 2239.00
Penetration (mbsf): 1508.00
Total number of cores: 122
Total length of cored section (m): 1003.2
Total core recovered (m): 865.99
Core recovery: 86.3%
Comments: Cores 118-735B-1D through 88N were recovered during Leg 118. Leg 176 coring began with Core 176-735B-89R and ended with Core 176-735B-210R.

INTRODUCTION

Leg 176 was devoted to the deepening and logging of Hole 735B atop a shallow bank along a transverse ridge at the Atlantis II Fracture Zone, Southwest Indian Ridge. There, 500 m of gabbro was cored 10 yr ago during Leg 118. During Leg 176, the hole was deepened more than 1000 m to a total depth of 1508 m before weather-related drill-string failure terminated coring. Fishing cleared some of the pipe from the

[1]Examples of how to reference the whole or part of this volume.
[2]Shipboard Scientific Party addresses.

Ms 176IR-101

hole, and logging was conducted in the upper 595 m. More igneous rock was recovered (some 865.99 m, representing 86.3% recovery) than on any previous Ocean Drilling Program (ODP) or Deep Sea Drilling Project (DSDP) leg. The combined results of drilling during Legs 118 and 176 make Hole 735B one of the most important accomplishments in the history of scientific ocean drilling. For the first time, a significant proportion of an all but inaccessible layer of the Earth's crust has been sampled in situ. We are now able to describe the architecture and outline the magmatic, structural, and metamorphic history of a block of the lower ocean crust, which formed at an ultra-slow-spreading ridge 11 m.y. ago.

Because of its inaccessibility, the nature of the lower ocean crust has been one of the longest standing questions in marine geology and has largely been inferred from remote sensing and analogy to on-land sections of fossil ocean crust (ophiolites). From the earliest seismic studies, the ocean crust has been believed to have an uncomplicated and uniform layered seismic structure (Hill, 1957; Raitt, 1963; Christensen and Salisbury, 1975). This structure was long equated to a simple layer-cake sequence, known as the Penrose model (Penrose Conference Participants, 1972; Coleman, 1977), of sediment, pillow basalt and diabase, and a thick gabbro section overlying the Earth's mantle, with the igneous crust/mantle boundary at or near the Moho. Accretion of the lower crust, in this model, resulted from crystallization from some form of near-steady-state magma chamber, or crystal mush zone, where magmas accumulate beneath a sequence of sheeted dikes and pillow lavas over the ascending mantle. Internally, a simple lower crustal stratigraphy was believed to exist, consisting of primitive layered gabbros overlain by more evolved isotropic gabbros, all of which were equated to seismic Layer 3.

Recent studies, however, indicate that the ocean crust has a more complex, three-dimensional structure that is dependent on magma supply and spreading rate and that large steady-state magma chambers are absent (e.g., Whitehead et al., 1984; Detrick et al., 1990; Bloomer and Meyer, 1992; Sinton and Detrick, 1992; Carbotte and Macdonald, 1992; Nicolas et al., 1996). This is particularly the case for slow-spreading ridges. Provision is now made for thinner crust near large transform faults or where half-spreading rates are significantly below 10 mm/yr (e.g., Reid and Jackson, 1981; Bown and White, 1994; Mutter and Detrick, 1984; Dick, 1989). Compilations of dredge results and seismic data show that a continuous gabbroic layer does not exist at slow-spreading ridges (Whitehead et al., 1984; Mutter et al., 1985; McCarthy et al., 1988; Dick, 1989; Cannat, 1993; Tucholke and Lin, 1994). Earlier drilling at Atlantis Bank and the Mid-Atlantic Ridge Kane Fracture Zone region (Leg 153; Cannat, Karson, Miller, et al., 1995) demonstrated that the internal stratigraphy of the lower ocean crust at slow-spreading ridges is governed as much by the dynamic processes of alteration and tectonism as by igneous processes. Finally, the abundance of serpentinized peridotite in dredge hauls from rift valley and fracture zone walls (Aumento and Loubat, 1971; Thompson and Melson, 1972; Fisher et al., 1986; Dick, 1989; Cannat, 1993) has again raised the possibility that serpentine can be a significant component of seismic Layer 3 as originally suggested by Hess (1962).

With this increasing complexity, in situ observation of the lower ocean crust by drilling is a necessity if the processes of ocean crust accretion and the nature of the ocean crust are ever to be understood. DSDP and ODP have previously sampled in situ ocean crust in a variety

of spreading environments to sub-bottom depths as great as 2 km. Although this has confirmed many inferences from ophiolites as to the shallow structure and composition of the ocean crust, it also has produced some unexpected results. Despite the recovery of short sections of lower ocean crust and mantle during several ODP legs, no truly representative section of seismic Layer 3 had ever been obtained in situ, leaving its composition, state of alteration, and internal structure almost entirely a matter of inference.

Hole 735B came close to achieving this goal with a 1508-m section of coarse gabbro drilled in a tectonically exposed lower crustal section on a wave-cut platform flanking the Atlantis II Fracture Zone on the slow-spreading Southwest Indian Ridge. The new results from Hole 735B, together with those from Leg 118, substantially change our perception of the lower ocean crust at slow-spreading ridges. The additional km of drilling documents a systematic variation in igneous petrology, structure, and alteration with depth quite unlike that associated with large magma chambers or even the melt lens now inferred to exist beneath fast-spreading ridges. It provides a first assessment of synkinematic igneous differentiation in which the upper levels of the gabbroic crust are enriched in late differentiated melts by means of tectonic processes, rather than simple gravitationally driven crystallization differentiation. Given the typical 4- to 6-km thickness of seismic Layer 3, this long section does not characterize the lower crust for all ocean basins. However, if the lower crust at ultra-slow-spreading ridges is only ~2 km thick, as predicted, then it is a beginning.

Overall, the sequence of rocks sampled in Hole 735B is unlike that in a Penrose-type ophiolite or in layered intrusions. Some of its attributes, including the lack of well-developed layering, and the presence of small 100- to 500-m intrusions, are similar to structural characteristics from ophiolites believed to have formed in slow-spreading environments, such as the Trinity or Josephine ophiolites. However, several of the major features of the section have not been described from these ophiolites. These include (1) the occurrence of innumerable discrete large and small, often sheared oxide-rich gabbros intruding undeformed olivine gabbro; (2) a striking downward decrease in abundance of oxide-rich gabbros through the section; (3) a baseline igneous stratigraphy of successive small "isotropic" olivine gabbro intrusions, the chemistries of which are less primitive in the lower kilometer of the hole; (4) the apparent synkinematic igneous differentiation of the section, with a concentration of late iron-rich melts near the top, apparently intruded along faults and shear zones; and (5) abundant crystal-plastic and brittle-ductile deformation at the top of the section that decreases downward. Together with the well-known geochemical affinities of many slow-spread ophiolites for the "arc-environment," most are not very good analogs for the Hole 735B section. Although an exact on-land counterpart may not exist, there are similarities to some Ligurian ophiolites, and more careful documentation of lower crustal sections in some ophiolites may reveal more similarities.

The Hole 735B gabbros correspond closely to those dredged and drilled at fracture zones and rift valley walls at slow-spreading ridges, and this, then, would seem to confirm the long-standing inference that the accretionary processes in the lower crust are highly sensitive to spreading rate. Gabbros from the East Pacific Rise drilled during Leg 147 at Hess Deep, and gabbros in ophiolites believed formed at fast-spreading centers (e.g., Oman), have an entirely different pattern of alteration (e.g., Dick et al., 1992; Manning and MacLeod, 1996) and lack the

extensive crystal-plastic fabrics of the Hole 735B gabbros. Moreover, the lack of well-defined, planar, and continuous igneous layering at Hole 735B also contrasts with layering in the lower two-thirds of the Oman section.

In basic outline, the gabbroic crust drilled over the two legs consists of five, possibly six, main blocks of relatively primitive olivine gabbro and troctolite, from 200 to 500 m thick, each with its own internal chemical and petrological coherence. Overall, each of these bodies appears to be composed of many smaller magma bodies. These probably represent small intrusions into solidified gabbro, where contacts are sharp, or into crystal mushes, where contacts are diffuse or sutured. Smaller crosscutting bodies of olivine gabbro and troctolite may represent feeder channels for melts migrating toward the surface or feeding intrusions higher in the section. Overall, each of the composite intrusions has more fractionated, oxide-bearing gabbros toward the top, and the most primitive and magnesian rocks, toward the base. Thus, each composite body likely represents a major cycle of magmatic intrusion and in situ differentiation as the melts worked their way upward through the section.

Although the boundaries of each of these principal intrusions are fairly well defined, the relationships of one to another are neither simple nor consistent. The uppermost intrusion is separated from the one underneath by a massive zone of Fe-Ti oxide-rich gabbro along a zone of shear. There is also a small, but abrupt, deformational offset between the lower two. There is a zone of brittle faulting near the contact between the second and third masses, but it is not at the contact. Instead, the contact, which is actually distributed over a zone of several tens of meters, appears to represent a series of crosscutting lithologies and to be intrusive in character overall. The presence of multiple composite intrusions, with large-scale repetitions of magmatic-crystallization sequences, confirms that this portion of the Southwest Indian Ridge was not supplied by a steady-state magma source.

Although about 80% of the Leg 118 and 176 cores are oxide-poor gabbro or olivine gabbro, these are crossed by numerous bodies of Fe-Ti oxide-bearing and Fe-Ti oxide-rich (ilmenite and titanomagnetite) gabbro, gabbronorite, and olivine gabbro. The largest body is a 70-m-thick zone of oxide olivine gabbro between 200 and 270 mbsf. Typically, however, they are only a few centimeters to a few tens of centimeters thick, with more than 600 identified by magnetic susceptibility measurements, using a multisensor track (MST), on the Leg 176 core alone. Many of the narrow oxide-rich zones have associated veins or small dikelets of siliceous diorite, trondhjemite, and granodiorite. The oxide-rich zones (and veins) diminish downhole from some 30% of the core in the upper 500 m, to 12% of the core in the subjacent 1000 m, and to less than 1% of the core in the lowest 300 m of the hole. These oxide gabbros represent the product of extended high-iron differentiation of parental basaltic liquids, and the thick sequences near the top of the hole must reflect complex processes of segregation from a large volume of rock. The uniform depletion of most of the Hole 735B cores of Ti and highly incompatible elements suggests that Fe-Ti rich liquids were expelled from their crystalline matrix by the interactive processes of crystallization and compaction in a dynamic environment. The tendency of oxide gabbros to be associated with zones of crystal-plastic deformation, and the presence of late magmatic oxides locally crosscutting crystal-plastic fabrics, suggests that the processes of aggregation

and transport of the late magmatic liquids were related to deformation and faulting of the gabbros before solidification.

Our structural observations demonstrate that crustal accretion at this ultra-slow-spreading ridge was strongly influenced by localized deformation from magmatic to low-temperature cataclastic conditions. High-temperature metamorphic effects are transitional to magmatic processes, and some, perhaps many, rocks were deformed and recrystallized while still partly molten. Some of the most striking zones of crystal-plastic deformation, however, apparently formed under the equivalent of granulite facies metamorphic conditions (>800°–1000°C), when there was little or no melt present. Although 77% of the gabbro contains no macroscopic magmatic or deformation fabric, and long sections of the core may be undeformed, there are numerous magmatic, crystal-plastic, and brittle deformation features, with a clear decrease in intensity vertically downward. Above 500 m the dominant sense of shear is normal, whereas below this there are several zones with numerous reverse-sense shears. A weak, subparallel, crystal-plastic fabric, which may record a transition from magmatic to crystal-plastic deformation, commonly overprints magmatic foliations. Many of the deformed rocks also show a continuum between crystal-plastic and brittle behavior. There are some narrow zones of intense cataclasis and several faults, two of which coincide with Leg 118 vertical seismic profile reflectors.

Overall, metamorphism and alteration of the Hole 735B cores can be portrayed as having occurred in two stages. Initially, alteration occurred under dynamic conditions, ranging from granulite to amphibolite, with only minor greenschist facies, beneath the rift valley and at the beginning of uplift and unroofing. This was followed by a lower temperature sequence, under relatively static conditions, representing block uplift to the summit of the transverse ridge and subsequent cooling to the present day. Whereas hydrothermal alteration to amphibole and sodic plagioclase is locally extensive in shear zones near the top of the section, it is minor below 600 m. Overall, static high-temperature alteration in undeformed gabbros is patchy, rather than pervasive. Extensive intervals (>300 m) have less than 10% background alteration, and the gabbro is generally very fresh. Whereas greenschist facies alteration is minor, likely reflecting rapid cooling from amphibolite-facies conditions during block uplift, lower-temperature alteration is more prominent. This is represented by the local formation of abundant late smectite, carbonate, and zeolite-prehnite veins, with iron oxyhydroxides, particularly in a zone of intense alteration between 500 and 600 mbsf. Deeper in the hole, there are also locally abundant smectite-lined fractures associated with sulfides, indicating formation under nonoxidative, low-temperature conditions.

Rock magnetic measurements show a consistent average stable inclination of ~71° in Hole 735B, with only minor downhole variation. The rocks have been tilted ~20° but have a very stable remanent magnetization and often very sharp blocking temperatures, suggesting relatively rapid acquisition of thermoremanence during cooling. This cooling occurred while the rocks were beneath the rift valley and relatively shortly after they crystallized. They thus constitute an ideal source for marine magnetic anomalies, and a gabbroic layer as thick as our drilled section is probably sufficient to account for the marine magnetic anomaly at Atlantis Bank over Hole 735B. Analysis of structures reoriented magnetically indicates that the dominant foliation dips preferentially toward the axial rift to the north.

TECTONIC SETTING

Introduction

Hole 735B is located adjacent to the Atlantis II Transform Fault on the ultra-slow-spreading Southwest Indian Ridge (Fig. F1). It was first described by Engel and Fisher (1975) and was mapped in detail by Dick et al. (1991b; Fig. F2). It is a 199-km, 20-m.y.-old north-south left-lateral ridge offset at 57°E. Although the spreading rate of the Southwest Indian Ridge has been fairly constant for the last 30 m.y. at 16 mm/yr (Fisher and Sclater, 1983), the transform lengthened at about 4 mm/yr because of asymmetric spreading at both ridge axes for at least the last 20 m.y. (Dick et al., 1991c). The transform valley is deep (up to 6480 m), with flanking transverse ridges shoaling to as little as 694 m (at Atlantis Bank). The walls are extremely steep, typically sloping from 25° to 40°, and are covered with extensive talus and debris. The transform floor has a >500-m-thick sequence of turbidites shed from the walls and is bisected by a 1.5-km-high median tectonic ridge. Extensive dredging shows that more than 80% of the crust exposed in the active transform valley and its walls is serpentinized peridotite, diabase, and gabbro, whereas only 16.3% is pillow basalt corresponding to the shallowest layer of the crust. By contrast, only relatively undisrupted pillow lavas appear to be exposed on crust along the non-transform walls of the inactive fracture zone valleys north and south of the present-day ridge axes (Dick et al., 1991c; e.g., Fig. F3).

Site Location

Hole 735B is located at 720 meters below sea level (mbsl) on Atlantis Bank, close to the crest of a 5-km-high transverse ridge that forms the eastern wall of the Atlantis II transform valley (Fig. F3A). It is 93 km south of the present-day ridge axis and 18.4 km from the inferred axis of transform faulting (Dick et al., 1991c). The Bank consists of a steep-sided flat-topped platform, roughly 9 km long north-south and 4 km wide. It is the shallowest of a series of uplifted blocks and connecting saddles that form the transverse ridge. The top of the platform has only ~120 m relief over ~25 km² above the 800-m contour (see **"Bathymetry of Atlantis Bank"** chapter, which is an oversized figure that accompanies this volume). The boundary between magnetic Anomalies 5r.2n and 5r.2r crosses east-west directly over the platform just north of Hole 735B (Fig. F4).

A 4-hr 200 m × 200 m video survey conducted near the hole during ODP Leg 118 (Fig. F5) shows a surface consisting of flat outcrops of foliated and jointed gabbro with minor relief, featureless sediment of undetermined but likely insignificant thickness, and basement with such a thin coat of sediment that outcrop textures were easily distinguished through it in the video image. The strikes of distinct joints and fractures estimated from the motion vector of the camera frame and the direction of ship motion, (with roughly 5°–10° error) are also indicated on the survey map (Fig. F5).

The generally east-west foliation around Hole 735B is roughly orthogonal to the transform and parallel to the ridge axis. When projected westward across the platform, it intersects a long oblique west-northwest–trending ridge coming up the wall of the fracture zone (Fig. F3A). Ridges produced by landslips and debris flows are normally oriented orthogonal to the fracture zone. Possibly this oblique ridge, and a

F1. Location of Atlantis II Fracture Zone, **p. 44.**

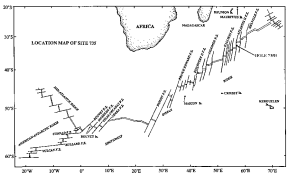

F2. Bathymetric map of Atlantis II Fracture Zone, **p. 45.**

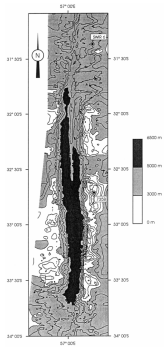

F3. Hand-contoured bathymetric map of Site 735, **p. 46.**

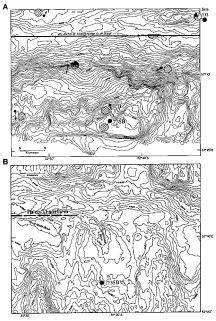

F4. Magnetic anomalies over Site 735, **p. 47.**

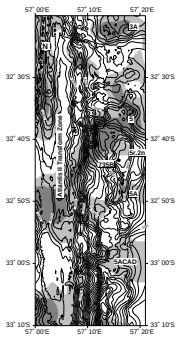

similar one 2 km to the north, represent the traces of inclined shear zones dipping to the north, exposed on the transform wall. Given the once shallow water depth, the canyon between these ridges may be an erosional remnant trough between resistant foliated gneissic amphibolites (Dick et al., 1991c). Assuming the ridge represents a shear zone, a three-point solution for the dip, based on an east-west strike, gives ~40°—close to the average for the amphibolite mylonites drilled in the upper 100 m of Hole 735B.

Well-defined magnetic anomalies cross over Atlantis Bank, and Site 735 is the only location in the ocean basins where the age of the magnetic anomaly (Anomaly 5r.2n, 11.75 Ma; Figs. **F2, F3, F4**) has been confirmed, within error, by a zircon U-Pb isotopic age date of 11.3 Ma from a trondhjemite sampled in situ (Stakes et al., 1991). Given the position of the site, the relatively constant spreading direction over the last 11 m.y., and the ridge-parallel strike of the local foliation, the Atlantis Bank gabbros must have accreted beneath the ridge axis 15 to 19 km from the ridge-transform intersection around 11.5 Ma. The smoothly domed, very nearly flat surface of the platform suggests that it formed by wave erosion of a small island created when the gabbros were unroofed and uplifted at the inside-corner high of the ancestral Southwest Indian Ridge at 11 Ma. The platform then subsided to its present depth by means of normal lithospheric cooling (Dick et al., 1991c). A similar wave-cut platform, from which rounded cobbles of peridotite have been dredged, exists on the Southwest Indian Ridge at the southern ridge-transform intersection of the DuToit Fracture Zone (Fisher et al., 1986).

The exposure and emplacement of the Hole 735B section likely occurred by unroofing at a long-lived detachment fault on the rift valley wall followed by block uplift into the inside-corner high at the ancestral ridge-transform intersection of the Atlantis II Fracture Zone (Fig. **F6;** Dick et al., 1991c). Similar exposures of plutonic rock have been found at several present-day ridge-transform intersections, most notably at the eastern inside-corner high of the Kane Fracture Zone in the Atlantic. There, as at the present-day northern ridge-transform intersection of the Atlantis II Fracture Zone, an intact volcanic carapace is found in the rift mountains on only one side of the rift valley, spreading in the direction away from the active transform. On the other side of the rift valley, deep crustal rocks and mantle peridotite are exposed on the rift valley wall at the inside-corner high. This remarkable asymmetry is well illustrated by comparing the seafloor topography around Hole 735B to that for crust of the same age situated on the opposite northern lithospheric flow line (Fig. **F3B**). This asymmetry is inferred to result from the periodic formation of a crustal weld between new ocean crust and the old cold lithospheric plate at the ridge-transform intersection. Because of this weld, the more rigid shallow levels of the newly formed ocean crust spread with the older plate in the direction away from the active transform. At depth, beneath the brittle–ductile transition, the plutonic section spreads symmetrically in both directions (Dick et al., 1981; Karson and Dick, 1983). At the Kane Fracture Zone, the surface of the detachment fault has been directly observed by submersible (Dick et al., 1981; Karson et al., 1987, Mével et al., 1991). Such detachment faults are suggested to form periodically by fault capture during amagmatic periods at slow-spreading ridges (Harper, 1985; Karson, 1990, 1991).

The ultra-slow-spreading rate of the Southwest Indian Ridge has important implications for crustal structure at Site 735. Although

F5. Outcrop map in vicinity of Hole 735B, **p. 48.**

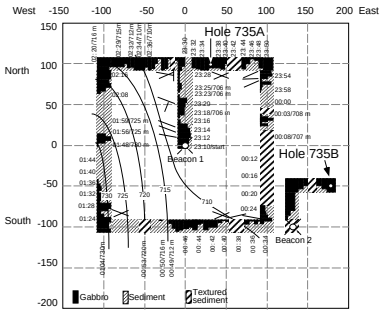

F6. Temporal cross sections of SWIR rift valley, **p. 49.**

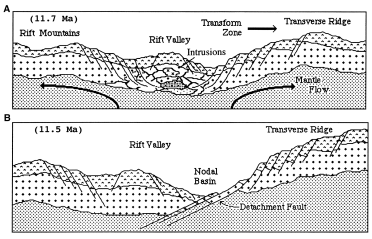

crustal thickness is roughly constant with spreading rate above a half rate of 10 mm/yr, it appears to drop off rapidly at slower rates (Reid and Jackson, 1981; Jackson et al., 1982). Seismic refraction measurements at both the Arctic and Southwest Indian Ridges indicate typical crustal thicknesses of ~4 km, including normal ocean crust immediately east of Hole 735B (Jackson et al., 1982; Bown and White, 1994; Minshull and White, 1996).

Muller et al. (1997) found that the seismic thickness of the crust north and south of Atlantis Bank is 4 km, with Layer 2 having a normal thickness of ~2 km (Fig. **F7**). Beneath Atlantis Bank, however, the depth to the Moho is 5 ± 1 km below the seafloor (Muller et al., 1997), despite the absence of either pillow lavas or sheeted dikes corresponding to seismic Layer 2. It is unlikely, in this environment, that this can all be igneous crust. In addition, mantle peridotites were dredged on the walls of the bank not far from Hole 735B at 4382 m, 1.3 km above the Moho (Dick et al., 1991c). Inversion of rare earth element concentrations in basalts dredged from the conjugate site to the north, exposing crust of the same age as Atlantis Bank, suggest a crustal thickness of 3 ± 1 km (Muller et al., 1997). Thus, Muller et al. (1997) agree with the geologic evidence (Dick et al., 1991c) that the crust is thin beneath Atlantis Bank and that the Moho there represents an alteration front in the mantle.

F7. Seismic velocity structure, **p. 51.**

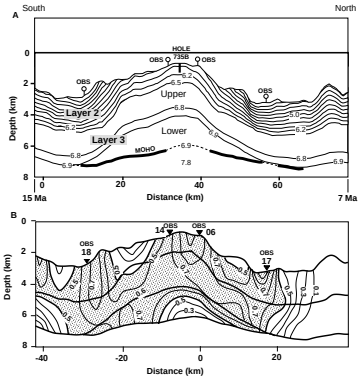

PREVIOUS RESULTS FROM HOLE 735B

Hole 735B was originally drilled during Leg 118 to a total reported depth of 500.7 m, recovering 435 m of olivine gabbro and oxide olivine gabbro and related rocks (Robinson, Von Herzen, et al., 1989). Subsequently, during reoccupation of the hole during Leg 176, the depth to the bottom of the hole was measured as 504.8 m before the resumption of drilling. Depth to seafloor was the same as during Leg 118, and there is no explanation for this discrepancy. The unanticipated volume and rate of recovery did not permit adequate time to fully describe the Hole 735B cores during Leg 118. A subset of the scientific party, including Dick, Meyer, Bloomer, Stakes, and Kirby with the help of Chris Mawer, redescribed the core at the Texas A&M repository (Dick et al., 1991a). The final igneous lithostratigraphy conforms in general to the original six units described in the *Initial Results* volume (Robinson, Von Herzen, et al., 1989). The precise boundaries of the principal units, however, were moved by as much as 2 m. The units were subdivided into a total of 12 different subunits, consisting of ~495 distinct igneous lithologic intervals. At the same time, a full inventory of all metamorphic veins, a new log of deformation intensity, and detailed structural measurements were made.

The Leg 118 cores largely consist of olivine gabbro with apparently minor cryptic chemical variations. There is little evidence of the process of magmatic sedimentation, which is important in layered intrusions. This body is crosscut by numerous small microgabbro intrusions ranging from troctolite to oxide gabbronorite as well as a suite of late felsic veins, principally trondhjemite. The microgabbros often have highly irregular, but sharp contacts with the olivine gabbro, suggesting assimilation-fractional crystallization processes accompanying upward intrusion of melt bodies through the section. Primitive troctolites and troctolitic microgabbros are relatively abundant at the base of the section (up to Fo_{87} olivine) and were (erroneously) believed to be a harbinger of a major body of troctolite intruding the olivine gabbro from

below. The olivine gabbro and microgabbros were in turn cross-intruded by numerous bodies of oxide-rich or oxide-bearing (0.1%–2%) gabbro, olivine gabbro, and gabbronorite. These are frequently associated with rock deformed during both hypersolidus and subsolidus conditions, during which late magmatic oxides filled cracks and formed pressure shadows around pyroxene augen. Geochemically, this produced an unusual extremely bimodal chemical variation with depth, without any first-order vertical variation in chemistry. This was unlike anything yet reported from a layered intrusion or ophiolite (see **"Igneous Petrology,"** p. 11).

These results were interpreted to show that the section formed by continuous intrusion and reintrusion of numerous small, rapidly crystallized bodies of magma (Bloomer et al., 1991; Dick et al., 1991c; Natland et al., 1991; Ozawa et al., 1991). Each batch of melt was intruded into a lower crust consisting of crystalline rock and semisolidified crystal mush. This led to undercooling and rapid initial crystallization of new magmas to form a highly viscous or rigid crystal mush, largely preventing the formation of magmatic sediments. Initial crystallization was followed by a longer, and petrologically more important, period of intercumulus melt evolution in a highly viscous crystal mush or rigid melt-crystal aggregate.

An unanticipated major feature of Hole 735B was the evidence for deformation and ductile faulting of still partially molten gabbro (Cannat, 1991; Dick et al., 1991a; Bloomer et al., 1991; Dick et al., 1992; Natland et al., 1991). This deformation was apparently particularly important over a narrow window late in the crystallization sequence (probably at 70%–90% crystallization) when the gabbros became sufficiently rigid to support a shear stress. This produced numerous small and large shear zones with enhanced permeability into which late intercumulus melt moved by compaction out of the relatively undeformed olivine gabbro (Dick et al., 1991a; Natland et al., 1991; Bloomer et al., 1991). Migration of this late iron-rich intercumulus melt into and along the shear zones locally hybridized the gabbro by melt-rock reaction and by precipitation of ilmenite, titanomagnetite, and other late magmatic phases. The net effect of these synchronous magmatic and tectonic processes is a complex igneous stratigraphy of relatively undeformed oxide-free olivine gabbros and microgabbros crisscrossed by bands of ferrogabbro. This process, also termed differentiation by deformation (Bowen, 1920), has recently been inferred for portions of the Lizard ophiolite (Hopkinson and Roberts, 1995). Evidence of such hypersolidus deformation is absent, however, in high-level East Pacific Rise gabbros drilled at Hole 894G at Hess Deep (Natland and Dick, 1996; MacLeod et al., 1996). Also, basalts corresponding to melts in equilibrium with the ferrogabbros of Hole 735B are absent along this region of the Southwest Indian Ridge, although some do erupt along the East Pacific Ridge. Therefore the late magmatic liquids that permeated the shear zones were evidently uneruptable throughout most of their crystallization.

The primary igneous assemblage recrystallized under granulite- to amphibolite-facies conditions, and this was accompanied by the formation of amphibole-rich shear zones (Cannat et al., 1991; Cannat, 1991; Dick et al., 1991a, 1992; Mével and Cannat, 1991; Stakes et al., 1991; Vanko and Stakes, 1991). Locally there is a strong association between amphibole veins and zones of intense deformation. At this stage, as during late magmatic conditions, formation of ductile shear zones appears to have localized late fluid flow, with the most intense alter-

ation occurring in or near zones of deformation. High-temperature alteration is far more extensive than found in layered intrusions (Dick et al., 1991a; Stakes et al., 1991), which are typically intruded and cooled in a near static environment. A rapid change in alteration conditions was seen in the Leg 118 gabbros, however, in the middle amphibolite facies with the virtual cessation of brittle-ductile deformation (Dick et al., 1991a; Stakes et al., 1991; Stakes, 1991; Vanko and Stakes, 1991; Magde et al., 1995). Mineral vein assemblages change from amphibole rich to diopside rich, reflecting different, more-reacted, fluid chemistries. Continued alteration and cooling to low temperature occurred under nearly static conditions, similar to those found at large layered intrusions. These changes were probably the result of an inward jump of the master fault at the rift valley wall. This transferred the section out of the zone of extension and lithospheric necking beneath the rift valley into a zone of simple block uplift at the inside-corner high of the Atlantis II Fracture Zone. Hydrothermal circulation, little enhanced by stresses related to extension, was greatly reduced, driven largely by thermal-dilation cracking as the section cooled to the current low temperatures in the hole.

The uniform stable magnetic inclination measured in Hole 735B gabbros drilled during Leg 118 demonstrates that there was little significant late tectonic disruption of the section, although the relatively steep inclination suggests block rotation of up to 20° (Pariso et al., 1991). The section thus likely preserves a typical record of accretion, hydrothermal circulation, and brittle-ductile deformation beneath an active rift. However, the later history of the rocks reflects static block uplift to shallow depths and rapid cooling at the ridge-transform intersection. Consequently, they do not record the full record of thermal equilibration and alteration of mature ocean crust cooled at depth beneath an intact section of ocean floor during seafloor spreading.

The Leg 118 results from Hole 735B show the importance of ephemeral magmatism, deformation, and alteration on crustal accretion at ultra-slow-spreading ridges. This contrasts with the results from the East Pacific Rise crustal section exposed at Hess Deep. There, no evidence of crystal-plastic deformation was found either in the high level gabbros from Hole 894G or in dredged gabbros (Gillis, Mével, Allan, et al., 1993)—perhaps because of the presence of a near-steady-state melt lens at the top of the section during accretion.

MAJOR OBJECTIVES ACCOMPLISHED DURING LEG 176

The major objectives of Leg 176 were to recover a representative section of gabbroic Layer 3 and determine its lithologic variation with depth. The operational goal was drilling to 1.5 km mbsf, with the hope that this would be deep enough to penetrate the crust/mantle boundary. Leg 176 met the operational goal and achieved the objective of obtaining a representative long section of the lower crust. The three to four intrusions drilled during Leg 176, however, are geochemically less primitive than those drilled in the upper 500 m of Hole 735B, and unlike the case at many ophiolites, no thick layered gabbro sequences were recognized. The absence of such features, which are often associated with the base of the crust in many ophiolites, suggests that we may still be relatively high in the section. Alternatively, there may be little

layered gabbro at the base of the crust here. The extent to which Hole 735B is representative of the igneous lower crust, then, depends on the evidence, discussed earlier, that the crust at Atlantis Bank is relatively thin, around 2 km, and the degree to which it has not been disrupted. With respect to the latter, the remarkably uniform magnetic inclination with depth and the systematic changes in the degree of alteration, nature of deformation, and rock chemistry described below all indicate that the section is not seriously disrupted or imbricated. Moreover, at the bottom of the hole during Leg 176, despite the less-primitive chemistry, we encountered rapidly increasing olivine contents and coarse troctolitic gabbros, which again raised hopes that we were near a major change in lithology, and perhaps were close to the crust/mantle boundary.

LEG 176 SCIENTIFIC RESULTS

Core Description

Description of the Hole 735B section required logging the features of 866 m of rock from a 1-km section of the lower ocean crust and integrating those observations with those made previously from the overlying 500-m section drilled during Leg 118. The recovery was more than double that of Leg 118, which previously held the record, and was some seven times the amount logged during Leg 147 in similar materials at Hess Deep. To accomplish this, the scientific party divided into specialist igneous, metamorphic, and structural teams, rather than into alternating watches. The teams, in turn, divided core description into specific tasks, with one individual responsible for logging a specific observation. This method proved remarkably efficient, generating more data, observations, and core descriptions than on any previous hard-rock drilling leg.

The greatest value of this approach, however, was a dramatic improvement between Legs 118 and 176 in consistency, precision, and accuracy of observation. For example, different individuals estimated the modal abundance of plagioclase, olivine, and pyroxene in each of the 457 discrete igneous intervals described, whereas modes were independently determined by point-counting 220 representative thin sections. Averaged for the hole, the macroscopic modal analysis gave 59.5% plagioclase, 30.1% augite, 8.8% olivine, 0.33% orthopyroxene, and 0.76% oxide; point counting gave 58.9% plagioclase, 30.6% augite, 8.2% olivine, 0.62% orthopyroxene, and 0.79% oxide. The difference in orthopyroxene abundances is because half of it occurs as rims around olivine and cannot be distinguished macroscopically. These consistent observations, in turn, allowed direct comparisons between independently observed features of the core. Oxide abundances, for example, logged on a centimeter scale down the entire core, proved to have a remarkable positive correlation with the degree of crystal-plastic and magmatic foliation. The combined observations greatly facilitated our interpretation of the evolution of the lower crust at Hole 735B.

Igneous Petrology

The Hole 735B core from between 504 and 1508 mbsf was divided by the igneous team into 457 discrete igneous intervals, numbered from 496 to 952 following the succession from the upper 500 m of Hole 735B

(Dick et al., 1991a). These were distinguished on the basis of igneous contacts, variations in grain size, and the relative abundances of primary mineral phases (Fig. **F8**). Individual contacts were then described and logged. The major lithologies in Hole 735B were gabbro and olivine gabbro, comprising 14.9 and 69.9 vol% of the core, respectively. The distinction between the two is arbitrary, set at 5% olivine following the classification of the International Union of Geological Sciences, and there is complete gradation between them. The separation, however, allowed distinction of areas of lesser olivine content in the core. Generally, these are equigranular rocks (Fig. **F9A**) that occasionally contain a weak magmatic foliation often overprinted by crystal-plastic deformation (Fig. **F9D**). Frequently, though, it is varitextured, with irregular coarse, medium, fine, and even pegmatitic patches (Fig. **F9E, F9F**).

The average grain size of samples varies from fine grained (<1 mm) to pegmatitic (>30 mm), with average grain sizes generally in the range of coarse (5–15 mm) to very coarse (15–30 mm). In general, the relative grain sizes for the major minerals are in the order augite > plagioclase > olivine, but are usually similar. Pegmatitic intervals are sporadic through the core (Fig. **F9E**). Peaks in average grain size occur at 510, 635, 825, 940, 1100, 1215, 1300, 1425, and 1480 mbsf, and the grain size data for augite, plagioclase, and olivine all follow similar trends.

Weak modal and grain size layering is present in 22 intervals (12 vol% of the core). The types of layering observed include (1) grain-size layering characterized by either sharp breaks in grain size or gradational variations in grain size (Fig. **F10A**), (2) modal layering marked by distinct changes in the abundance of plagioclase, olivine, clinopyroxene, and Fe-Ti oxide (Fig. **F10B, F10C**), (3) magmatic foliation (igneous lamination) defined by the preferred orientation of plagioclase and in some cases olivine and clinopyroxene, and (4) layering defined by textural changes such as layers with crescumulus texture. In several intervals, grain-size and modal layering are present in rhythmic sequences.

The olivine gabbro is locally crosscut by fine- to medium-grained microgabbros having contacts that range from sharp, with a slight but definable finer-grained margin, to irregular grading and swirling up through and into the adjoining olivine gabbro (Fig. **F9B**). These range in composition from primitive troctolites in lithologic Units IV and XII at the top and bottom of the Leg 176 section, to microgabbro and gabbronorite, although the majority are olivine microgabbros, which are nevertheless similar to the olivine gabbros they frequently cut. The origin of these bodies is speculative, as they could represent channels along which relatively hot primitive melt was fed up into the succession of gabbro intrusions, or they could be protodikes through which the typically primitive magmas of the Southwest Indian Ridge erupted to the seafloor.

Oxide-rich gabbros, including oxide olivine gabbro, make up 7 vol% of the recovered rocks, and gabbronorites and oxide gabbronorites make up approximately 8 vol%. These intervals range considerably in size, but they decrease noticeably downward in the section and never are as abundant as the upper 500 m of the hole. There is nothing like the nearly 100-m-thick polygenetic units of disseminated oxide olivine gabbro and oxide olivine gabbro containing numerous sheared intervals in Units III and IV between 170.22 and 274.06 mbsf. The latter requires that a very large flux of melt passed through them to account for the massive precipitation of intercumulus Fe-Ti oxides (Natland et al., 1991; Dick et al., 1991a), whereas the former could easily have crystallized from locally derived iron-rich melts sweated out of the crystal-

F8. Lithostratigraphic column, **p. 52.**

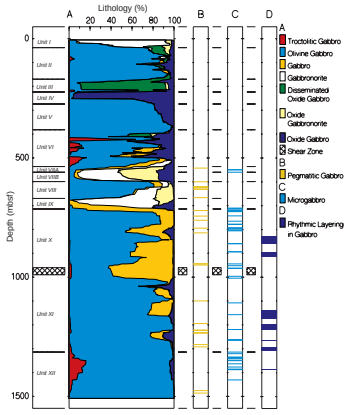

F9. Close photographs of cored gabbro, **p. 53.**

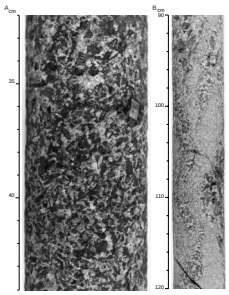

F10. Representative layered sections of Leg 176 core, **p. 56.**

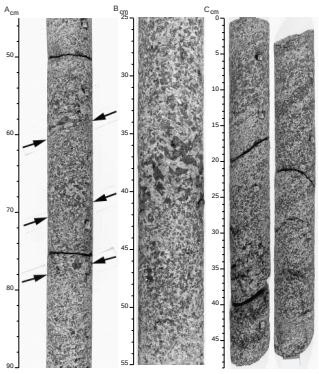

lizing olivine gabbros. The oxide-rich gabbros in the lower two-thirds of Hole 735B are found as innumerable sheared and undeformed irregular patches and veins in olivine gabbro (Fig. F9C) and as consistently deformed larger intervals each as thick as several meters or more. A consistent and impressive feature of the oxide gabbros is their overall strong association with areas of magmatic and crystal-plastic foliation, as detailed in the structure section, and with the percent oxide found in the core. This is noteworthy because most of these rocks are cumulates and do not represent a liquid composition. Moreover, the liquids with which they were in equilibrium were far more evolved than any pillow basalt that has been dredged along the Southwest Indian Ridge (Natland et al., 1991; Dick et al., 1991a).

Dick et al. (1991a) proposed that this is because the oxide gabbros represent intrusion of late iron-rich melts that have migrated out of the olivine gabbros and along shear zones penetrating or originating in partially molten lower crust (synkinematic igneous differentiation). When such melts migrate upsection and down a temperature gradient, they should decrease in mass as they migrate and crystallize. In the case of a late Fe-Ti-rich melt near the end of crystallization migrating through gabbros sufficiently rigid to support a shear stress (80%–90% crystallinity), the liquid would precipitate abundant ilmenite and magnetite as it cooled. Thus, the greater the fluid flux through any volume, the greater should be the enrichment in precipitated oxides. Accordingly, the association between oxides and deformation throughout Hole 735B can be interpreted as evidence that deformation and the formation of shear zones influenced the flow and transport of late intercumulus melt throughout the section.

A wide variety of felsic rocks constituting 0.5% of the core were described. The majority are leucodiorite; however, diorite, trondhjemite, tonalite, and very little granite also are present. They are largely net veins, and rarely are sufficiently massive (5 cm) to be described as an igneous interval. Although many of these veins are clearly of igneous origin, having primary igneous textures and sharp intrusive contacts, many have experienced subsequent high- and low-temperature alteration and developed diffusive or reactive contacts with the host gabbros. Still others may be hydrothermal or metamorphic in origin.

Seven additional major lithologic units (VI through XII) were identified below the Leg 118 section. These are based on modal mineralogy and the relative abundance of rock types and include Unit VI—compound olivine gabbro, which continues from 382 mbsf in the Leg 118 core to 536 mbsf; Unit VII—gabbronorite and oxide gabbronorite from 536 to 599 mbsf; Unit VIII—olivine gabbro from 599 to 670 mbsf; Unit IX—gabbronorite and gabbro from 670 to 714 mbsf; Unit X—olivine gabbro and gabbro from 714 to 960 mbsf; Unit XI—olivine gabbro from 960 to 1314 mbsf; and Unit XII—olivine gabbro and troctolitic gabbro from 1314 mbsf to the bottom of the drilled hole at 1508 mbsf. These units are shown in Figure F8. The stratigraphy, at first glance, would seem to resemble that of a large layered intrusion, with the proportion of rocks crystallized from differentiated and evolved liquids increasing upward. However, this is misleading. There is little layering, and none that resembles that characteristic of a layered intrusion. Rather, the section consists of a series of individual olivine gabbro intrusions, best defined geochemically, which are crosscut repeatedly at higher levels in the crust by oxide-rich gabbros. Thus the lower ocean crust here is differentiated kinematically by intrusion of late melts into the top of the section. In fact, as discussed in the

geochemistry section, despite irregularly increasing olivine content, the lower olivine gabbros are less primitive, more titanian and richer in soda, than those crosscut by the evolved intrusives higher in the section.

The average phase proportions in Hole 735B troctolites and olivine gabbros closely resemble cotectic proportions observed in low-pressure experiments on mid-ocean-ridge basalts, suggesting that the main body of olivine gabbro crystallized at relatively shallow depths (<6 km) and solidified after efficient expulsion of residual melts. The more evolved Fe-Ti oxide-bearing gabbros do not have good experimental cotectic analogs. The strong correlation between deformation and oxide-rich gabbros in the section suggests (1) lenses of late-stage magma may have acted as zones of weakness along which deformation was concentrated; (2) late-stage magmas may have been concentrated in zones that had been previously sheared, because these zones have greater high-temperature permeability; or (3) active shear zones acted as conduits for melt transport through the section. The high concentrations of oxides present in some samples require that large volumes of melt were transported through these zones.

Metamorphic Petrology

The metamorphic petrology team logged 2792 veins as well as groundmass alteration assemblages on a piece-by-piece basis downcore. This was supplemented by an examination of some 243 thin sections of the Leg 176 cores. The individual observations were made by two pairs of investigators, with one pair identifying, measuring, and logging veins and the other characterizing and logging alteration in the groundmass of the gabbros. The same types of observations, and others, were then made on the thin-section suite by a fifth investigator, who separately confirmed and expanded the observations of the macrodescription teams. In hand sample, plagioclase alteration was based on the extent of a milky white appearance. This did not distinguish between hydrothermally altered plagioclase and plagioclase recrystallized by the high-temperature granulite facies deformation, which was pervasive in many sections of the core. Thus the total background alteration logged downhole is significantly greater than might be inferred in thin sections, in which secondary plagioclase that formed during hydrothermal alteration is more readily distinguished from that produced by dynamic recrystallization. However, such a distinction is often arbitrary and was not made here. Otherwise, the thin-section observations are remarkably consistent with the observations of alteration in hand specimen. The thin-section observations are presented in Figure **F11**. Total alteration and vein abundances downhole are plotted in Figure **F12**. This figure uses additional data on vein abundances for the upper 500 m (Dick et al., 1991a).

The gabbros recovered during Leg 176 range from fresh to 40% altered, although there are many small intervals where alteration is far more extensive. Typically, however, there is less than a few percent total hydrothermal alteration through long sections. The most intensely altered portion of the core is between 500 and 600 mbsf, where both amphibole and secondary recrystallized plagioclase are most abundant and the primary minerals are on average 10% to 40% replaced. This contrasts sharply with the amphibolite mylonites at the top of Hole 735B, where total alteration was more intense, coming close to 100% (e.g., Robinson et al., 1991; Stakes et al., 1991). Calcite veins, associated

F11. Downhole distribution of secondary phases, p. 57.

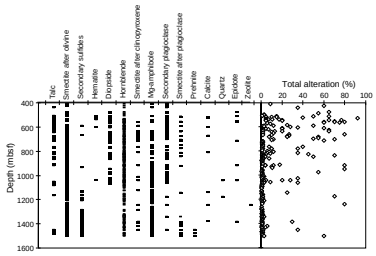

F12. Distribution of veins, Legs 118, 176, p. 58.

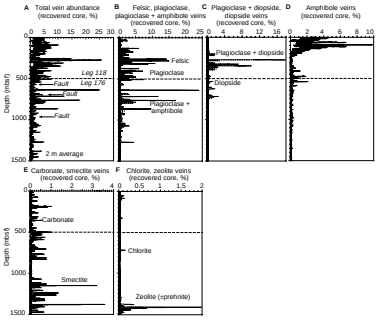

with low-temperature oxidation of the rocks, are also abundant between 500 and 600 m, evidently reflecting ongoing alteration at low temperatures as a result of the presence of open fractures. A second zone of intense recrystallization is present between 800 and 1030 mbsf, where many of the rocks exhibit high-temperature plastic deformation, and veins are rare. Two less altered zones are located in an interval of abundant smectite veins at 1300–1500 mbsf. Below 1030 m, the intensity of alteration is generally much less than 10%.

The Leg 176 gabbros preserve a complex record of high-temperature metamorphism, brittle failure, and hydrothermal alteration that began at near-solidus temperatures and continued down to very low-temperature conditions. The highest temperature metamorphic effects are transitional with magmatic processes; they most likely overlap both temporally and spatially, and in places the effects of these two processes are nearly indistinguishable. This is particularly true of the felsic vein assemblages, which range from clearly magmatic to apparently exclusively hydrothermal. Plagioclase and diopside veins, and combinations thereof, on splays from apparently igneous felsic veins were not unusual (Fig. **F13**). In general, felsic veins also served as conduits for late fluids, possibly of magmatic origin, commonly leaving a heavy overprint on the igneous assemblages, and which extended to partial replacement of some veins with clays.

F13. Plagioclase and diopside veins, **p. 59.**

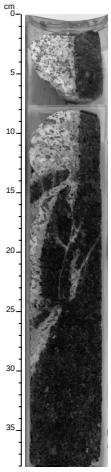

Granulite facies metamorphic conditions (>800°–1000°C) are clearly marked by localized, narrow zones of crystal-plastic deformation that cut igneous fabrics. These intervals characteristically have anastomosing layers of olivine and pyroxene neoblasts that are bounded by plagioclase-rich bands. In some places, the high-temperature shear zones are associated with impregnations of oxide gabbros; in many cases, these zones have abundant recrystallized brown hornblende, indicating that deformation continued down to amphibolite facies metamorphic conditions. Other high-temperature effects probably resulting from late-stage magmatic activity include the formation of plagioclase + amphibole veins and diopside-rich veins, which in some intervals are progressively transposed into localized zones of high-temperature shear. Many of these rocks, veins, and shear zones reflect the effects of late magmatic hydrous fluids, but these zones also acted as pathways for later hydrothermal fluids at various temperatures.

Static high-temperature alteration is commonly associated with vein formation, and it is patchy throughout the section. Extensive intervals (>300 m) are marked by less than 10% total background alteration. This alteration is generally manifested by coronitic alteration halos around olivine grains, and the common replacement of clinopyroxene by variable amounts of brown amphibole. In more evolved rocks, magnesium-amphibole ± talc typically replaces orthopyroxene. The secondary minerals most likely formed under low water-to-rock ratios over a range of temperature, from >600° to 700°C down to much lower temperatures.

Ingress of very warm to hot fluids (400°–550°C) was facilitated by subvertical fractures, now lined with amphibole, that were probably related to cooling and cracking of the rocks in the subaxial environment (e.g., Fig. **F14**). However, the abundance of amphibole veins decreases markedly with depth, as does the alteration, and below 600 mbsf amphibole veins are rare. Amphibole veins and groundmass alteration are associated with zones of deformation at the top and bottom of the Leg 118 portion of the hole, with a sharp drop in abundance in undeformed intervals. The greatest alteration, often with complete replacement of mafic phases by amphibole and the highest vein abun-

F14. Subvertical amphibole vein, **p. 60.**

dances, is situated in the upper 100 m in a zone of intense deformation (Dick et al., 1991a; Stakes et al., 1991). A second, more irregular zone of deformation and alteration is present from 400 to 500 mbsf, where amphibole replacement of mafic phases is only partial. Although this zone of deformation and associated amphibole alteration continues into the upper 100 m of the Leg 176 section, it does not reach deeper levels of the core, where foliated gabbros largely experienced crystal-plastic deformation at high temperatures. Microcracks filled with talc, magnetite, amphibole, sodic plagioclase, chlorite, and epidote are sporadically present throughout the core and represent smaller scale fracturing and fluid penetration under greenschist facies metamorphic conditions.

Cessation of hydrothermal fluid flow is marked by abundant late smectite, carbonate, zeolite ± prehnite veins and iron oxyhydroxide minerals associated with intense alteration at 500–600 mbsf. These minerals reflect low-temperature alteration by circulating seawater solutions, and they are most likely related to the presence of a fault at 560 mbsf. Smectite veins (Fig. **F15**), unlike the higher temperature vein assemblages, are often associated with alteration haloes where olivine and even pyroxene are extensively replaced by smectite. Below this interval, veins of smectite ± pyrite ± calcite, together with associated smectitic alteration of surrounding wallrock, reflect low-temperature hydrothermal reactions under more reducing conditions. These effects are observed throughout much of the core, but the abundant smectite veins at 600–800 m are most likely related to another fault at 690 mbsf. This lower temperature set of veins formed in tensional fractures and is most likely related to cooling of the block during uplift of the massif to form the transverse ridge.

A peculiar feature of the Hole 735B cores is that high-temperature alteration assemblages are most abundant at the top of the section, whereas low-temperature assemblages dominate near the base. Greenschist assemblages, representing intermediate conditions, are relatively minor. This inversion of the normal order of things, which has, for example, been found in the in situ section of sheeted dikes and pillow lavas at Hole 504B (Alt, Kinoshita, Stokking, et al., 1993), is reasonably attributed to the particular cooling history of the section. Apparently, at an early stage, conditions for the percolation of water to great depth did not exist beneath the rift valley, and alteration was largely limited to the upper portions of the gabbroic crust. Before a normal cooling profile could be established, however, the massif was unroofed and rapidly uplifted to the seafloor. The rapid cooling and relatively static conditions in the interior of the uplifted block inhibited extensive greenschist facies alteration, and there is only a single large epidote vein found in the entire lower two-thirds of the hole. In contrast, low-temperature alteration phases are abundant in the lower two-thirds of the core. This likely reflects alteration in the rift mountains after unroofing and uplift of the gabbro massif. With re-establishment of a normal conductive geotherm, circulation of seawater through a relatively restricted set of open fractures and continued cracking resulting from cooling produced local zones of oxidative alteration and smectite-lined veins.

F15. Vein of pale-green smectite, p. 61.

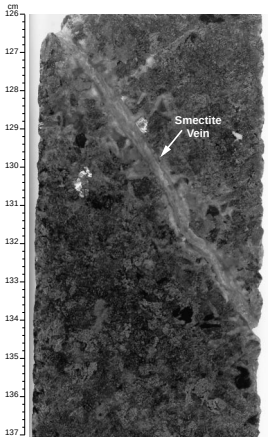

Geochemistry

To represent a systematic sampling of the major lithologies in the Leg 176 cores, 180 whole-rock samples were selected for analysis, represent-

ing one analysis every 4.8 m of recovered core. In principle, at least one sample representing the main lithology was taken from each core, even when an apparently homogeneous unit spanned several cores. Seams of oxide gabbro and larger felsic veins were occasionally sampled to study the complete range of petrologic differentiation. Given the distribution of lithologies, the large majority of the samples chosen for analysis were olivine gabbros and subordinate gabbro, disseminated Fe-Ti gabbro, and microgabbros. A limited number of samples were selected from the intervals strongly affected by high- and low-temperature alteration. Of the 458 igneous intervals identified in the core, about 140 are represented in the analysis suite. Analysis was done using X-ray fluorescence (XRF) for major element compositions and for the abundances of the trace elements V, Cr, Ni, Cu, Zn, Rb, Sr, Y, Zr, and Nb. Sample preparation techniques are outlined in the "Explanatory Notes" chapter. Samples taken for analysis generally weighed 20 to 30 g. Larger slabs were cut from the very coarse-grained intervals, and a thin section was prepared from a billet from the same or adjacent material. A representative selection of analyses for the different lithologies is included in Table T1.

Figures F16, and F17, show the downhole variation of Mg# and TiO_2. The least evolved rocks are troctolites from 500–520 mbsf. Throughout the entire gabbro section there are numerous thin intervals of Fe-Ti oxide gabbros and felsic veins that are significantly to strongly differentiated. The Mg# should be used with some caution as a "differentiation index" in the case of the oxide gabbros. Mg#s of cumulate rocks decrease as a result of the accumulation of iron-rich minerals, such that low numbers overestimate the extent of crystallization. Overall, the gabbros are split into two groups. The most voluminous are olivine gabbros and troctolites with minor oxides that have high magnesium numbers. These are crosscut by later Fe-Ti-rich oxide gabbros and felsic veins with high TiO_2 contents, low Mg#, and relatively sodic compositions that exhibit extreme variability in their composition because of the accumulation of iron oxides. Such narrow, crosscutting late rock types are of little value in establishing a chemical stratigraphy, which is based entirely on the chemistries of the main gabbro types and principally on the Mg#s. Examining the depth profile (Fig. F16), approximately five major cycles can be identified of decreasing Mg# going from high Mg at depth to low Mg with increasing TiO_2 in the olivine gabbros (roughly 0–225, 250–525, 525–900, 950–1350, and 1350–1508 mbsf). A prominent feature of the observed variation is that the lowermost three units in this cyclic repetition are more iron rich than the upper two; this is consistent with a somewhat more sodic composition and a slightly higher TiO_2 content of the rocks.

As seen in Figure F8, the most extreme lithologic variability exists in the upper 1000 m of the hole, with the lowermost 500 m being largely olivine gabbro. Within the upper kilometer there is also an apparent change in the proportions of different lithologies above and below 500 mbsf. A preliminary mass balance calculation using the measured thickness of the lithologies, their average compositions from the shipboard XRF measurements, and the average rock densities, shows that the bulk composition of the 500–1000 m interval has 0.69 wt% TiO_2, 2.99 wt% Na_2O, and a Mg# of 70.5. By contrast, the same calculation done for the 0–500 m interval (Dick et al., 1991a) gives a bulk composition with 1.41 wt% TiO_2, 2.67 wt% Na_2O, and a Mg# of 67.2. Although the 0–500 m interval is richer in titanium and has a lower Mg# than the 500–1000 m section, it also has lower Na_2O, which appears inconsistent with the

T1. Averaged chemical compositions of samples from Hole 735B, p. 70.

F16. Mg# vs. depth for Hole 735B, p. 62.

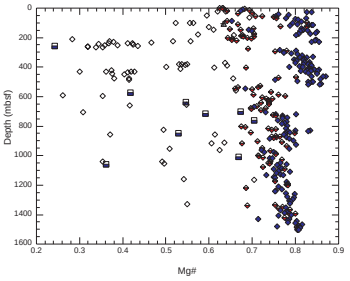

F17. TiO_2 vs. depth in Hole 735B, p. 63.

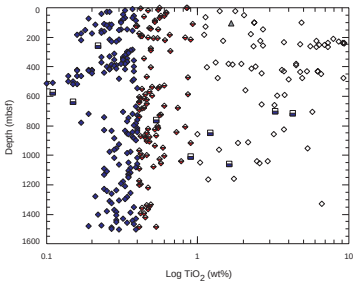

hypothesis that it simply crystallized from more evolved liquids. In fact, the olivine gabbros in the uppermost 500 m are more primitive than those in the middle 500 m (0.34 wt% TiO_2, 2.49 wt% Na_2O, 80.3 Mg# vs. 0.43 wt% TiO_2, 2.87% wt% Na_2O, and 71.6 Mg#). This difference in the bulk chemistry between 0–500 m and 500–1000 m (which would be even more pronounced with a comparison to the largely olivine gabbro 1000–1508 m section) is entirely due to the increasing volume of intrusive Fe-Ti oxide-rich gabbros and gabbronorites in the upper part of the hole.

The main conclusions that can be drawn from the shipboard chemical analyses from both Legs 176 and 118 are as follows:

1. The main rock type is a moderately fractionated olivine-bearing gabbro having between 0.2 and 1.0 wt% TiO_2. Fe-Ti oxide gabbros containing up to 7 wt% TiO_2 and up to 20 wt% Fe_2O_3 are present in centimeter- to decimeter-thick intervals throughout the core. The abundance of Fe-Ti oxide appears to decrease with depth, but this is not related to a decrease in TiO_2 of the parental liquids from which the gabbros crystallized. The development of localized concentrations of Fe-Ti-rich gabbro seems to depend on favorable conditions for formation rather than on the TiO_2 content of the starting material.
2. Gabbros with similar Mg#, MgO, and Ni contents but variable TiO_2 content commonly occur together. Hence the differences in TiO_2 content cannot result from simple fractional crystallization from a common parental magma. Factors other than cotectic crystallization affected phase proportions and compositions. These are likely to include complex mixing of early cumulates with more differentiated liquids, assimilation-fractional crystallization processes during melt transport through the mass, and redistribution of crystal phases during solution channeling of migrating melts.
3. Within the 1000-m section drilled during Leg 176, four chemical units can be identified, the uppermost of which is a continuation of one drilled during Leg 118. With few exceptions the boundaries of these units coincide with changes in lithologic, metamorphic, and structural properties. The thickness of the separate units varies from 100 to 300 m. Most likely these chemical units represent the scale at which individual magmatic events added to the construction of oceanic Layer 3 at this ultra-slow-spreading ridge.

Structural Geology

Measurements made on the Leg 176 core by the structural team include intensity and orientation of magmatic deformation, crystal-plastic deformation, cataclastic deformation, igneous and metamorphic veins, as well as description of crosscutting relationships. Additional observations on thin sections were made as a team with the aid of a video monitor. The results showed considerable variation in the structures observed throughout Hole 735B, both in style and position. Several unexpected features, notably the occurrence of significant reverse-sense shear zones and a general decrease in deformation downhole, were found.

Wherever possible, observations on the Leg 176 cores were combined with results from the upper 500 m of the hole drilled during Leg 118.

This was done using published results, and by combining our observations with data logs for the intensity and orientation of deformation and metamorphic veins for the Leg 118 section used by Dick et al. (1991a). The team also relogged the lowermost 50 m of the core recovered during Leg 118 to provide a basis for comparison of the Leg 176 observations to those for the upper 500 m of the hole.

The structural geologists marked all the Leg 176 cores orthogonal to the foliation for splitting. The cores were placed into the archive and working halves of split core liners with the foliation dipping in the 90° direction in the core reference frame (i.e., dipping to the right on the cut face of the core in the working half). This provided a consistent framework for description and measurement of structures in the core. Thus the strong local concentration of poles to foliation shown in the stereo plots in Figure F18 with respect to strike are a direct artifact of the method in which they were split and oriented in the core liners. They are not geographically referenced. However, shipboard paleomagnetic declinations for these cores show a similar cluster around 250° in the core reference frame throughout the entire cored interval. This result demonstrates that, overall, the foliations have a consistent orientation and thus can be reoriented into the geographical reference frame by making the assumption that the declination of the remanent magnetic vector dips toward the south. The resulting reorientation suggests that both the crystal-plastic and the late magmatic foliations predominantly dip to the north and, hence, toward the ridge axis.

F18. Magmatic foliation, stereoplots, and photomicrographs, p. 64.

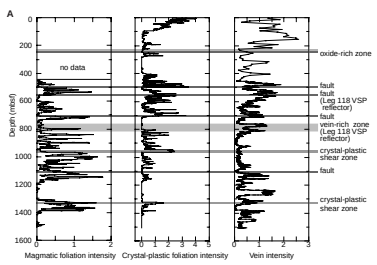

Macroscopic Observations

A majority of the rocks from Hole 735B (78%) have coarse- to medium-grained hypidiomorphic-granular, intergranular, and subophitic textures with no preferred mineral alignment caused by late magmatic deformation. The remainder contain a variably developed magmatic foliation that is defined by the preferred orientation of elongate plagioclase laths and, locally, by pyroxene crystals with weak magmatic foliations predominating and strong fabrics occurring sporadically (Fig. F18). Magmatic foliations vary in strike and dip, with no systematic variation with depth. The majority have dips between 20° and 50°.

Crystal-plastic deformation in Hole 735B, as shown in Figure F18. It is highly localized, with the most intense deformation observed in the intervals 0–50 and 450–600 mbsf, and with intervals of little or no crystal-plastic deformation generally increasing in number and length downhole. Overall, 77% of the rocks recovered during Leg 176 have no crystal-plastic fabric, and only 7% have more than a weak foliation, whereas 71% of the Leg 118 gabbros have no crystal-plastic fabric and 14% have more than a weak foliation. Again, there is no systematic variation of the dip of the foliation with depth, although there is a strong concentration at ~30°.

A striking feature of the crystal-plastic deformation fabrics from Hole 735B is the number of shear zones with reverse sense of shear concentrated within and below the 20-m-wide shear zone between 945 and 964 mbsf and above the fault at 690 mbsf. From the top of the core to 680 mbsf, the majority of the shear zones display normal shear. An example of a reverse shear zone is shown in Figure F19. These are as yet unexplained; however, the high temperature of their formation, and the origin of the Atlantis Bank at the inside-corner high, dictate that

F19. Close-up photo of reverse fault, p. 66.

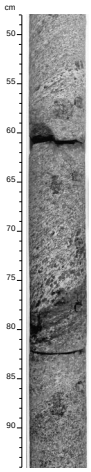

shear zones formed in the lower crust beneath the ancestral rift valley on the Southwest Indian Ridge.

A major feature of the Leg 176 cores is the strong association between magmatic and crystal-plastic fabrics (Fig. F18A). This is striking because only 22% of the core has a weak to moderate magmatic foliation, and less than 1% a strong magmatic foliation, whereas 77% of the gabbro has no crystal-plastic fabric at all. Obviously, no magmatic fabric should be preserved in regions with a strong crystal-plastic fabric (e.g., 710–730 mbsf); however, rocks with both fabrics are quite common and are always near each other and long intervals of the core contain neither. In addition, in areas where the crystal-plastic fabric is intense, a magmatic fabric is often observed in the adjacent gabbro. Because the two fabrics have similar orientations (Fig. F18B), it is evident that they developed under the same or similarly oriented stress fields. These observations indicate that crystal-plastic deformation localized within areas with a magmatic foliation, representing the transition from late magmatic to solid-state deformation. There are several interesting exceptions to this correlation, particularly in the lower portion of the hole, demonstrating that the relationship between the two may be complex in detail. The question naturally arises as to whether the "magmatic foliation" was truly produced by magmatic processes. This was addressed by a careful, independent assessment of 240 thin sections for the presence of crystal-plastic deformation and magmatic fabrics. Although weak magmatic fabrics are hard to see in thin section, undeformed samples with magmatic fabrics and the relative intensity of crystal-plastic fabric correlated remarkably well to the macroscopic observations of the core.

Retrograde shear zones at less than granulite facies conditions are evidenced by brittle-ductile deformation and the formation of amphibole in the plane of shear and by crosscutting veins and microcracks. Two principal retrograde shear zones are present in Hole 735B, both of which coincide with zones of earlier late magmatic deformation and crystal-plastic deformation. The most intense of these is in the upper 100 m of the hole, where pyroxene is often entirely replaced by amphibole and true amphibolites are found. The less intense zone is around 500 mbsf at the bottom of the Leg 118 section and the top of the Leg 176 section.

Lower temperature cataclastic fabrics and faults are found at several levels within the Leg 176 section and at the base of the Unit IV Massive Oxide Gabbro at 274 mbsf (Dick et al., 1991a). Potentially major faults are absent in the upper 450 m of the hole. Two relatively major faults with the potential for significant displacement (e.g., hundreds of meters to kilometers) exist at 560 and at 690–700 mbsf, in addition to several minor ones at different locations. Smaller discrete planar faults with associated gouge, breccia, cataclasite, and ultracataclasite cut all rock types. These were logged at 600 locations in the Leg 176 core but are concentrated in the upper half of the hole, and are virtually absent below about 1400 m. The most common of these features are small-offset microfaults filled with calcite, amphibole, and/or smectite (below 1050 mbsf). Mineral assemblages associated with the brittle tectonic structures include amorphous silica, prehnite, chlorite, epidote, actinolite, and secondary plagioclase. These reflect a range of conditions for cataclastic deformation. Downhole dip shows no consistent pattern, although there is a maximum of poles to foliation near a plunge of 90° in stereo plots indicating a preferred subhorizontal fault orientation in

the lower 1000 m of Hole 735B. Of the faults, 8.8% exhibit oblique slip, 2.8% are pure dip slip, and 2.3% are strike slip.

Summary of Structural Evolution of Hole 735B

The cores from Hole 735B contain many late brittle deformation features with evidence of cataclasis, which are associated with alteration assemblages extending from the lower greenschist facies to the current temperatures in the hole. These features are almost certainly associated with block uplift, unroofing, and subsequent cooling of the massif at the inside-corner high of the Southwest Indian Ridge. This in large part reflects the bimodal metamorphic history of the massif wherein low-temperature alteration is concentrated near the bottom of the hole, whereas high-temperature amphibolite-facies rocks are concentrated at the top.

The gabbroic rocks cored during Leg 176 display magmatic, crystal-plastic, and brittle deformation features together with associated overprinting relations consistent with synkinematic cooling and extension in a mid-ocean-ridge environment. The following observations provide a basis for interpreting the conditions of deformation during evolution of this block of lower oceanic crust.

1. Thick intervals of the core (up to ~150 m) are comparatively free of deformation and are either isotropic or contain local intervals with weak to moderate magmatic foliation; such intervals are most prevalent at the bottom of the hole. Magmatic foliations are often overprinted by a weak, parallel crystal-plastic fabric that may record the transition from magmatic to crystal-plastic deformation.
2. Numerous high-temperature reverse-sense shear zones are present in the interval between 900 and 1100 mbsf, including a 30-m-thick shear zone, and these are cut by lower temperature crystal-plastic or semi-brittle shear zones (~1–10 cm thick).
3. Felsic magmatic breccias and veins are abundant throughout the upper 1100 m and decrease in abundance toward the bottom of the hole.
4. The transition from crystal-plastic to lower temperature brittle deformation is associated with hydrothermal alteration at amphibolite to transitional greenschist-facies conditions.
5. Intense cataclasis is extremely localized downhole into zones of variable thickness up to centimeters thick.
6. Veins show a wide variation in abundance and a general decrease in dip downhole; steeply dipping amphibole veins are common down to 800 mbsf; moderately dipping smectite veins dominate between 800 and 1500 mbsf.
7. There is a strong correlation between sections rich in magmatic Fe-Ti oxides and regions with strong crystal-plastic deformation. The relationship between crystal-plastic deformation and the concentration of oxide-rich zones, however, is not unique. Macro- and microstructural observations indicate that (1) oxide-rich zones exist as late-crystallizing interstitial material, (2) oxide-rich zones are frequently spatially associated with faults and crystal-plastic shear zones, (3) lower temperature crystal-plastic and cataclastic deformation locally overprints some oxide zones, (4) concentrations of magmatic oxides locally cut high-temperature crystal-plastic fabrics along shear zones, and (5) many mag-

matic oxide-bearing shear zones cut through oxide-poor undeformed gabbros.

8. Based on thickness and fracture intensity of recovered cataclastic rocks, there are important zones (560 mbsf and 690–700 mbsf) and several minor zones (including 490, 1076, and 1100–1120 mbsf) of cataclasis. The sense and magnitude of displacement on these faults is unknown; however, they probably are associated with uplift of the Atlantis Bank crustal block.

These observations indicate that the processes that control crustal accretion at slow-spreading ridges are strongly influenced by localized deformation at conditions ranging from magmatic to low-temperature cataclastic. The correlation between structural domains and igneous intervals suggests that this segment of the Southwest Indian Ridge is not supplied by a steady-state magma source. Rather, intrusion and deformation are episodic phenomena that may occur separately or synchronously but at different rates. In many cases, zones of localized deformation remain active over a wide range of conditions, for example, cataclastic overprint of oxide-rich crystal-plastic shear zones that were initially active under partially molten conditions.

Paleomagnetism

Paleomagnetic intensities, inclinations, and declinations were measured separately on all the archive halves of the Leg 176 cores and on a large number of minicores drilled from the working halves. The average natural remanent magnetization (NRM) intensity of the Leg 176 minicores is 2.5 A/m, the same as the estimated value of 2.5 A/m for the upper 500 m of Hole 735B once the drilling-induced component is removed (Pariso and Johnson, 1993). There appears to be no general decrease in magnetization downhole; however, magnetic susceptibilities vary from 8.12×10^{-4} to 0.123 SI, with mean values smaller than for gabbros from the upper 500 m of the hole and having less scatter and decreasing slightly with depth (Fig. F20). Magnetic "hardness" increases with decreasing grain size and compensates for the strong decrease in abundance of relatively coarse-grained oxide gabbro downhole. Although olivine gabbro is nearly oxide free in the upper 500 m (Natland et al., 1991), it has significantly more relatively fine-grained Fe-Ti oxides in the lower 1000 m of Hole 735B, where it is the most abundant lithology. Overall, the gabbros of Hole 735B have a very stable remanent magnetization, with a high and often very sharp blocking temperature suggesting relatively rapid acquisition of thermoremanence during cooling of the gabbros.

The vertical structure of the sources of lineated marine magnetic anomalies has remained poorly known ever since the recognition, more than 30 yr ago, that the ocean crust records reversals of the Earth's geomagnetic field. Several authors have suggested that some or most of the stable source might reside in the gabbroic crust, based on the magnetization of dredged gabbros (Fox and Opdyke, 1973; Kent et al., 1978). However, such surficial samples have been subjected to varying degrees of hydrothermal alteration and weathering during faulting and emplacement to the seafloor that would likely significantly affect their magnetic properties. During the site survey for Leg 118 (Dick et al., 1991c), well-defined magnetic anomalies were mapped over large regions of the rift mountains of the Southwest Indian Ridge adjacent to the transform fault. Extensive dredging of these regions, including

F20. NRM, susceptibility, and inclination for Hole 735B, p. 67.

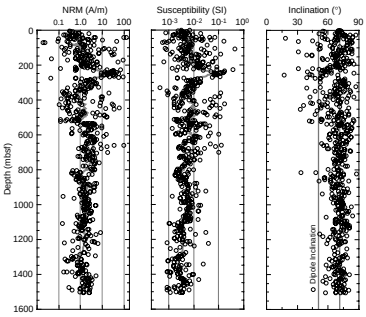

Atlantis Bank, recovered largely gabbro and peridotite, suggesting that these lithologies must be responsible for the anomalies (Dick et al., 1991c), a possibility first raised by the laboratory work of Fox and Opdyke (1973) and Kent et al. (1978). The hypothesis that gabbro could be a major contributor to the magnetic anomaly over Site 735 was confirmed by downhole logging (Pariso et al., 1991) and by direct measurements on cores (Kikawa and Pariso, 1991; Kikawa and Ozawa, 1992; Pariso and Johnson, 1993). With the addition of the Leg 176 cores, however, it now appears that the 1.5-km Hole 735B gabbro section is the principal source of the lineated magnetic anomaly over the site, to the extent that this section is representative of the crust in three dimensions.

This conclusion presents the possibility that gabbroic crust may potentially contribute to, and even exceed, the contribution of pillow basalts and sheeted dikes to marine magnetic anomalies elsewhere. However, the rapid acquisition of thermal remanence of the Hole 735B gabbros is consistent with rapid cooling caused by unroofing and uplift to sea level at the ridge-transform intersection. This may not be the case for normal Southwest Indian Ridge crust away from transforms, which would cool under a 2-km carapace of pillow basalts and sheeted dikes and acquire its thermal remanence more slowly.

Thermal and alternating field demagnetization studies of discrete samples from Leg 176 reveal two magnetization components: a low-stability component apparently related to drilling and more stable components with a steeper inclination. The mean characteristic inclination for Leg 176 discrete samples is reversed, with Inc = 71.4° (+0.3°/–3.1°), uncorrected for any hole deviation from vertical (Fig. **F20**). This is statistically identical to that found in the upper 500 m (71.3°, +0.4°/–11.0°) when the latter are recalculated using the method of McFadden and Reid (1982). Because Antarctica has been relatively fixed in the plate reference frame over the last 11 m.y., the present latitude of Hole 735B is likely close to that of the its ancestral ridge axis at the time of remanence acquisition. Thus, the observed inclination is steeper than the expected 52° for the site and requires a tectonic rotation of the section of approximately 19° ± 5° (depending on the deviation of the hole from vertical).

Overall, the tight cluster of stable magnetic inclinations downhole is significant to the interpretation of the igneous petrology and structure of Hole 735B, because the inclinations indicate that there has been little tectonic disruption of the section since it cooled below the Curie point at ~580°C. Moreover, there is an unexpected strong preferred orientation of declinations at ~260° in the reference frame of the core liner. This is because the structural geologists systematically oriented each section of core for splitting so that they were cut orthogonal to the foliation, with each half placed in the working and archive halves so that the foliation dipped consistently in one direction. Thus, the consistent declinations demonstrate that these foliations are not random and suggest that gross reorientation of structural features in the core may be possible. Assuming a south-pointing characteristic remanence declination, the mean declination of 260° would be restored to 180° by a counterclockwise rotation of ~80°. Structural planar features that preferentially dip toward 90° in the core reference frame would thus dip toward the axial rift to the north.

Physical Properties and Downhole Measurements

Physical properties were measured using the MST on all the whole cores (natural gamma ray, gamma-ray densiometry, and magnetic susceptibility). Also measured were index properties including density, porosity, compressional wave velocity, and thermal conductivity on archive-half core pieces and on minicores from the working half. Only the magnetic susceptibility measurements made on the MST proved to have geologic value.

Thermal conductivity measurements were made at 219 intervals through the borehole section. Over the section the thermal conductivity is 2.276 ± 0.214 W/(m·K). The thermal conductivity varied considerably in the region of felsic veins. These values lie within the range measured for the upper 500 m of Hole 735B and for gabbroic rocks in general (Clark, 1966).

Magnetic Susceptibility

The MST system measured in excess of 22,000 magnetic susceptibility points. These are shown in Figure F21 and exhibit two characteristic features. The first is an overall decrease in susceptibility downhole defined largely by a gradual decrease in the baseline value with depth. The second is the occurrence of more than 600 extreme spikes of high susceptibility that can be individually correlated to the location of intervals of oxide-rich gabbros and gabbronorites enclosed within oxide-poor olivine gabbro and crosscutting felsic veins in the Hole 735B cores. The MST spikes indicate that the typical interval is no more than 10 to 15 cm thick, and is in many cases significantly smaller. These intervals should be most abundant in the upper 500 m of the core, where susceptibility measurements on individual samples define the highest overall unit susceptibility, but where the MST measurements were not made. The proportion and frequency of these oxide-rich intervals decrease systematically downhole from 274 m at the base of the Unit 4 massive oxide olivine gabbro.

F21. MST log of magnetic susceptibility, p. 68.

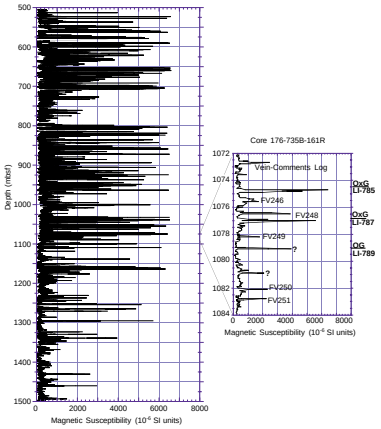

Density

Mass and volumetric measurements were made on 218 minicores with a mean porosity of 0.649% ± 2.884% (the population being heavily skewed by the large number of minimal porosities and the small number of porosities significantly greater than 1%). The mean bulk density was 2.979 ± 0.10 g/cm³, and a mean grain density was 2.991 ± 0.107 g/cm³, close to the density of the typical olivine gabbro (2.96 g/cm³). Density varied with mineral content and was highest in oxide gabbros (3.21 g/cm³) due to the presence of substantial ilmenite and magnetite (4.7–5.2 g/cm³) and lowest in troctolitic gabbros and olivine gabbros, where the proportion of plagioclase (2.7 g/cm³) was greatest. Density variations downhole are consistent (Fig. F22) with lithologic variations, with the greatest scatter in the upper 500 m where oxide gabbros are most abundant (between 2.8 and 3.3 g/cm³). Densities show increasing scatter below 925 mbsf (between 2.8 and 2.9 g/cm³). A slight decrease in mean density at the bottom of the hole reflects an increasing proportion of plagioclase-rich olivine gabbro and troctolite.

F22. Bulk density, velocity, and percent recovery, p. 69.

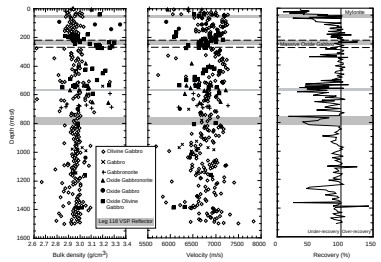

Vertical Incidence Seismic Profile Reflectors

The physical properties measurements provide considerable insight into the origin of the vertical incidence seismic profile (VSP) reflectors identified from the Leg 118 VSP (Swift et al., 1991). The compressional velocities of 217 minicores were measured; they averaged 6777 ± 292 m/s and are shown together with the data from Leg 118 in Figure F22. No significant variation in minicore compressional velocities occurs for the Leg 176 cores downhole, not even at the VSP reflectors at 560 m and between 760 and 825 m. Higher in the hole, however, there is a clear dip in velocities for the massive oxide gabbro Unit 4 that corresponds to a striking increase in the density of minicores and the vertical-incidence seismic profile reflector at 225–250 mbsf (Iturrino et al., 1991; Dick et al., 1991a). A sharp increase in seismic velocity of the Leg 118 cores near the top of the hole occurs in the vicinity of another reflector at 50 m. The latter corresponds to a zone of amphibolites with intense shear and crystal-plastic deformation that has produced a strong crystal-fabric orientation. Iturrino et al. (1991) demonstrated that these are elastically anisotropic, with strong directional variations in V_p related to foliation. The reflector is located at a break in the deformed interval where highly deformed amphibolites are juxtaposed against relatively undeformed gabbro.

The absence of a break in density or compressional *P*-wave velocity corresponding to the two lower VSP reflectors (560 and 760–825 m) demonstrates that these do not result from the intrinsic physical properties of the gabbros, whether the development of a strong preferred mineral fabric, or variations in density. Rather, they must correspond to another effect such as the presence of faults and fractures. This is confirmed by examination of the recovery record from Hole 735B (Fig. F22). Recovery in both massive fine- and coarse-grained, foliated and unfoliated gabbros was high, generally close to 100% in Hole 735B. Drilling rates, however, varied considerably in these lithologies, dropping dramatically for fine-grained intervals. Although the low recovery at the top of the hole likely reflects lack of drill-string stability, elsewhere, where the rocks are believed to be highly fractured, drilling rates increased dramatically, and recovery dropped to as low as 31%. The precise coincidence of the two lower VSP reflectors with intervals of dramatically reduced recovery, therefore, apparently confirms the hypothesis that these are highly fractured zones of rock corresponding to some form of faulting associated with the late uplift of the platform.

Downhole Measurements

The downhole measurements performed at the end of the leg show that there are distinct boundaries between each of the top six lithostratigraphic units of Hole 735B. Logging data also suggest that there are two faults centered at approximately 555 and 565 mbsf which are 2 and 4 m thick, respectively. These log measurements show reduced velocities, densities, resistivities, and elevated porosities at these intervals. These zones also correlate with the approximate depth of a seismic reflector identified during the Leg 118 VSP experiment. Data from the Formation MicroScanner (FMS) processed postcruise show a marked improvement over the initial raw data obtained at the end of the leg. Preliminary analysis shows that several hundred structural features strike generally west-northwest from 280° to 310°. The dip azimuth of these features ranges from 340° to 20° with several features also dipping

from 180° to 220°; the magnitudes mostly range from 10° to 50°. However, the degree to which the high concentration and magnetization of the oxide minerals influence the FMS magnetometer, which is essential to orient the structures observed in the FMS log throughout the upper 600 m of Hole 735B, is not yet known. Preliminary reorientation of core pieces shows a good correlation between Leg 118 borehole televiewer downhole tool data, digital unrolled core images, and Leg 176 FMS logs. A steep fracture dipping to the west is clearly identified in Core 118-735B-77R (403.5–409.5 mbsf) and the oriented logs.

REFERENCES

Alt, J.C., Kinoshita, H., Stokking, L.B., et al., 1993. *Proc. ODP, Init. Repts.,* 148: College Station, TX (Ocean Drilling Program).

Aumento, F., and Loubat, H., 1971. The Mid-Atlantic Ridge near 45°N. XVI. Serpentinized ultramafic intrusions. *Can. J. Earth Sci.,* 8:631–663.

Bloomer, S.H., and Meyer, P.S., 1992. Mid-ocean ridges; slimline magma chambers; discussion. *Nature*, 357:117–118.

Bloomer, S.H., Meyer, P.S., Dick, H.J.B., Ozawa, K., and Natland, J.H., 1991. Textural and mineralogic variations in gabbroic rocks from Hole 735B. *In* Von Herzen, R.P., Robinson, P.T., et al., *Proc. ODP, Sci. Results,* 118: College Station, TX (Ocean Drilling Program), 21–39.

Bowen, N.L., 1920. Differentiation by deformation. *Proc. Nat. Acad. Sci.,* 6:159–162.

Bown, J.W., and White, R.S., 1994. Variation with spreading rate of oceanic crustal thickness and geochemistry. *Earth Planet. Sci. Lett.,* 121:435–449.

Cande, S.C., and Kent, D.V., 1995. Revised calibration of the geomagnetic polarity timescale for the Late Cretaceous and Cenozoic. *J. Geophys. Res.,* 100:6093–6095.

Cannat, M., 1991. Plastic deformation at an oceanic spreading ridge: a microstructural study of Site 735 gabbros (southwest Indian Ocean). *In* Von Herzen, R.P., Robinson, P.T., et al., *Proc. ODP, Sci. Results,* 118: College Station, TX (Ocean Drilling Program), 399–408.

————, 1993. Emplacement of mantle rocks in the seafloor at mid-ocean ridges. *J. Geophys. Res.,* 98:4163–4172.

Cannat, M., Karson, J.A., Miller, D.J., et al., 1995. *Proc. ODP, Init. Repts.,* 153: College Station, TX (Ocean Drilling Program).

Cannat, M., Mével, C., and Stakes, D., 1991. Normal ductile shear zones at an oceanic spreading ridge: tectonic evolution of Site 735 gabbros (southwest Indian Ocean). *In* Von Herzen, R.P., Robinson, P.T., et al., *Proc. ODP, Sci. Results,* 118: College Station, TX (Ocean Drilling Program), 415–429.

Carbotte, S., and Macdonald, K., 1992. East Pacific Rise 8°′10°30′N: evolution of ridge segments and discontinuities from SeaMARC II and three-dimensional magnetic studies. *J. Geophys. Res.,* 97:6959–6982.

Christensen, N.I., and Salisbury, M.H., 1975. Structure and constitution of the lower oceanic crust. *Rev. Geophys. Space Phys.,* 13:57–86.

Clark, S.P. (Ed.), 1966. *Handbook of Geophysical Constants*. Mem.—Geol. Soc. Am., 97.

Coleman, R.G., 1977. *Ophiolites: Ancient Oceanic Lithosphere:* New York (Springer-Verlag).

Detrick, R.S., Mutter, J.C., Buhl, P., and Kim, I.I., 1990. No evidence from multichannel seismic reflection data for a crustal magma chamber in the MARK area on the Mid-Atlantic Ridge. *Nature,* 347:61–64.

Dick, H.J.B., 1989. Abyssal peridotites, very slow spreading ridges and ocean ridge magmatism. *In* Saunders, A.D., and Norry, M.J. (Eds.), *Magmatism in the Ocean Basins*. Geol. Soc. Spec. Publ. London, 42:71–105.

Dick, H.J.B., Bryan, W.B., and Thompson, G., 1981. Low-angle faulting and steady-state emplacement of plutonic rocks at ridge-transform intersections. *Eos,* 62:406.

Dick, H.J.B., Meyer, P.S., Bloomer, S., Kirby, S., Stakes, D., and Mawer, C., 1991a. Lithostratigraphic evolution of an in-situ section of oceanic Layer 3. *In* Von Herzen, R.P., Robinson, P.T., et al., *Proc. ODP, Sci. Results,* 118: College Station, TX (Ocean Drilling Program), 439–538.

Dick, H.J.B., Robinson, P.T., and Meyer, P.S., 1992. The plutonic foundation of a slow-spreading ridge. *In* Duncan, R.A., Rea, D.K., Weissel, J.K., von Rad, U., and Kidd, R.B. (Eds.), *The Indian Ocean: A Synthesis of Results from the Ocean Drilling Program*. Geophys. Monogr., Am. Geophys. Union, 70:1–50.

Dick, H.J.B., Schouten, H., Meyer, P.S., Gallo, D.G., Berg, H., Tyce, R., Patriat, P., Johnson, K., Snow, J., and Fisher, A., 1991b. Bathymetric map of the Atlantis II

Fracture Zone, Southwest Indian Ridge. *In* Von Herzen, R.P., Robinson, P.T., et al., *Proc. ODP, Sci. Results,* 118: College Station, TX (Ocean Drilling Program), foldout map.

Dick, H.J.B., Schouten, H., Meyer, P.S., Gallo, D.G., Bergh, H., Tyce, R., Patriat, P., Johnson, K.T.M., Snow, J., and Fisher, A., 1991c. Tectonic evolution of the Atlantis II Fracture Zone. *In* Von Herzen, R.P., Robinson, P.T., et al., *Proc. ODP, Sci. Results,* 118: College Station, TX (Ocean Drilling Program), 359–398.

Engel, C.G., and Fisher, R.L., 1975. Granitic to ultramafic rock complexes of the Indian Ocean Ridge system, western Indian Ocean. *Geol. Soc. Am. Bull.,* 86:1553–1578.

Fisher, R.L., Dick, H.J.B., Natland, J.H., and Meyer, P.S., 1986. Mafic/ultramafic suites of the slowly spreading southwest Indian Ridge: Protea exploration of the Antarctic Plate Boundary, 24°E'47°E. *Ophioliti,* 11:147–178.

Fisher, R.L., and Sclater, J.G., 1983. Tectonic evolution of the southwest Indian Ocean since the mid-Cretaceous: plate motions and stability of the pole of Antarctica/Africa for at least 80 Myr. *Geophys. J. R. Astron. Soc.,* 73:553–576.

Fox, P.J., and Opdyke, N.D., 1973. Geology of the oceanic crust: magnetic properties of oceanic rocks. *J. Geophys. Res.,* 78:5139–5154.

Gillis, K., Mével, C., Allan, J., et al., 1993. *Proc. ODP, Init. Repts.*, 147: College Station, TX (Ocean Drilling Program).

Harper, G.D., 1985. Tectonics of slow spreading mid-ocean ridges and consequences of a variable depth to the brittle/ductile transition. *Tectonics,* 4:395–409.

Hess, H.H., 1962. History of ocean basins. *Geol. Soc. Am., Buddington Vol.,* 599–620.

Hill, M.N., 1957. Recent geophysical exploration of the ocean floor. *Phys. Chem. Earth,* 2:129–163.

Hopkinson, L., and Roberts, S., 1995. Ridge axis deformation and coeval melt migration within layer 3 gabbros: evidence from the Lizard Complex. *U.K. Contrib. Mineral. Petrol.,* 121:126–138.

Iturrino, G.J., Christensen, N.I., Kirby, S., and Salisbury, M.H., 1991. Seismic velocities and elastic properties of oceanic gabbroic rocks from Hole 735B. *In* Von Herzen, R.P., Robinson, P.T., et al., *Proc. ODP, Sci. Results,* 118: College Station, TX (Ocean Drilling Program), 227–244.

Jackson, H.R., Reid, I., and Falconer, R.K.H., 1982. Crustal structure near the Arctic mid-ocean ridge. *J. Geophys. Res.,* 87:1773–1783.

Karson, J.A., 1990. Seafloor spreading on the Mid-Atlantic Ridge: implications for the structure of ophiolites and oceanic lithosphere produced in slow-spreading environments. *In* Malpas, J., Moores, E.M., Panayiotou, A., and Xenophontos, C. (Eds.), *Ophiolites: Oceanic Crustal Analogues:* Proc. Symp. "Troodos 1987": Nicosia, Cyprus (Minist. Agric. Nat. Resour.), 547–555.

————, 1991. Accommodation zones and transfer faults: integral components of Mid-Atlantic Ridge extensional systems. *In* Peters, U.J., Nicolas, A., and Coleman, R.G. (Eds.), *Ophiolites Genesis and Evolution of Oceanic Lithosphere:* Dordrecht (Kluwer Academic), 21–37.

Karson, J.A., and Dick, H.J.B., 1983. Tectonics of ridge-transform intersections at the Kane Fracture Zone. *Mar. Geophys. Res.,* 6:51–98.

Karson, J.A., Thompson, G., Humphris, S.E., Edmond, J.M., Bryan, W.B., Brown, J.R., Winters, A.T., Pockalny, R.A., Casey, J.F., Campbell, A.C., Klinkhammer, G., Palmer, M.R., Kinzler, R.J., and Sulanowska, M.M., 1987. Along-axis variations in seafloor spreading in the MARK area. *Nature,* 328:681–685.

Kent, D.V., Honnorez, B.M., Opdyke, N.D., and Fox, P.J., 1978. Magnetic properties of dredged oceanic gabbros and source of marine magnetic anomalies. *Geophys. J. R. Astron. Soc.,* 55:513–537.

Kikawa, E., and Ozawa, K., 1992. Contribution of oceanic gabbros to sea-floor spreading magnetic anomalies. *Science,* 258:796–799.

Kikawa, E., and Pariso, J.E., 1991. Magnetic properties of gabbros from Hole 735B, Southwest Indian Ridge. *In* Von Herzen, R.P., Robinson, P.T., et al., *Proc. ODP, Sci. Results,* 118: College Station, TX (Ocean Drilling Program), 285–307.

MacLeod, C.J., Boudier, F., Yaouancq, G., and Richter, C., 1996. Gabbro fabrics from Site 894, Hess Deep: implications for magma chamber processes at the East Pacific Rise. *In* Mével, C., Gillis, K.M., Allan, J.F., and Meyer, P.S. (Eds.), *Proc. ODP, Sci. Results,* 147: College Station, TX (Ocean Drilling Program), 317–328.

Magde, L.S., Dick, H.J.B., and Hart, S.R., 1995. Tectonics, alteration and fractal distribution of hydrothermal veins in the lower ocean crust. *Earth Planet. Sci. Lett.,* 129:103–119.

Manning, C.E., and MacLeod, C.J., 1996. Fracture-controlled metamorphism of Hess Deep gabbros, Site 894: constraints on the roots of mid-ocean-ridge hydrothermal systems at fast-spreading centers. *In* Mével, C., Gillis, K.M., Allan, J.F., and Meyer, P.S. (Eds.), *Proc. ODP, Sci. Results,* 147: College Station, TX (Ocean Drilling Program), 189–212.

McCarthy, J., Mutter, J.C., Morton, J.L., Sleep, N.H., and Thompson, G.A., 1988. Relic magma chamber structures preserved within the Mesozoic North Atlantic crust? *Geol. Soc. Am. Bull.,* 100:1423–1436.

McFadden, P.L., and Reid, A.B., 1982. Analysis of paleomagnetic inclination data. *Geophys. J. R. Astron. Soc.,* 69:307–319.

Mével, C., and Cannat, M., 1991. Lithospheric stretching and hydrothermal processes in oceanic gabbros from slow-spreading ridges. *In* Peters, T., Nicolas, A., and Coleman, R.J. (Eds.), *Ophiolite Genesis and Evolution of the Oceanic Lithosphere.* Petrol. Struct. Geol., 5:293–312.

Mével, C., Cannat, M., Gente, P., Marion, E., Auzende, J.-M., and Karson, J.A., 1991. Emplacement of deep crustal and mantle rocks on the west median valley wall of the MARK area (MAR 23°N). *Tectonophysics,* 190:31–53.

Minshull, T.A., and White, R.S., 1996. Thin crust on the flanks of the slow spreading Southwest Indian Ridge. *Geophys. J. Int.,* 125:139–148.

Muller, M.R., Robinson, C.J., Minshull, R.S., and Bickle, M.J., 1997. Thin crust beneath ocean drilling program borehole 735B at the Southwest Indian Ridge? *Earth Planet. Sci. Lett.,* 148:93–108.

Mutter, J.C., and Detrick, R.S., 1984. Multichannel seismic evidence for anomalously thin crust at Blake Spur fracture zone. *Geology,* 12:534–537.

Mutter, J.C., and North Atlantic Transect (NAT) Study Group, 1985. Multichannel seismic images of the oceanic crust's internal structure: evidence for a magma chamber beneath the Mesozoic Mid-Atlantic Ridge. *Geology,* 13:629–632.

Natland, J.H., and Dick, H.J.B., 1996. Melt migration through high-level gabbroic cumulates of the East Pacific Rise at Hess Deep: the origin of magma lenses and the deep crustal structure of fast-spreading ridges. *In* Mével, C., Gillis, K.M., Allan, J.F., and Meyer, P.S. (Eds.), *Proc. ODP, Sci. Results,* 147: College Station, TX (Ocean Drilling Program), 21–58.

Natland, J.H., Meyer, P.S., Dick, H.J.B., and Bloomer, S.H., 1991. Magmatic oxides and sulfides in gabbroic rocks from Hole 735B and the later development of the liquid line of descent. *In* Von Herzen, R.P., Robinson, P.T., et al., *Proc. ODP, Sci. Results,* 118: College Station, TX (Ocean Drilling Program), 75–111.

Nicolas, A., Boudier, F., and Ildefonse, B., 1996. Variable crustal thickness in the Oman ophiolite: implication for oceanic crust. *J. Geophys. Res.,* 101:17941–17950.

Ozawa, K., Meyer, P.S., and Bloomer, S.H., 1991. Mineralogy and textures of iron-titanium oxide gabbros and associated olivine gabbros from Hole 735B. *In* Von Herzen, R.P., Robinson, P.T., et al., *Proc. ODP, Sci. Results,* 118: College Station, TX (Ocean Drilling Program), 41–73.

Pariso, J.E., and Johnson, H.P., 1993. Do lower crustal rocks record reversals of the Earth's magnetic field? Magnetic petrology of gabbros from Ocean Drilling Program Hole 735B. *J. Geophys. Res.,* 98:16013–16032.

Pariso, J.E., Scott, J.H., Kikawa, E., and Johnson, H.P., 1991. A magnetic logging study of Hole 735B gabbros at the Southwest Indian Ridge. *In* Von Herzen, R.P., Robinson, P.T., et al., *Proc. ODP, Sci. Results,* 118: College Station, TX (Ocean Drilling Program), 309–321.

Penrose Conference Participants, 1972. Penrose field conference on ophiolites. *Geotimes,* 17:24–25.

Raitt, R.W., 1963. The crustal rocks. *In* Hill, M.N. (Ed.), *The Sea—Ideas and Observations on Progress in the Study of the Seas* (Vol. 3): *The Earth Beneath the Sea:* New York (Wiley-Interscience), 85–102.

Reid, I., and Jackson, H.R., 1981. Oceanic spreading rate and crustal thickness. *Mar. Geophys. Res.,* 5:165–172.

Robinson, P.T., Dick, H.J.B., and Von Herzen, R.P., 1991. Metamorphism and alteration in oceanic layer 3: Hole 735B. *In* Von Herzen, R.P., Robinson, P.T., et al., *Proc. ODP, Sci. Results,* 118: College Station, TX (Ocean Drilling Program), 541–552.

Robinson, P.T., Von Herzen, R., et al., 1989. *Proc. ODP, Init. Repts.,* 118: College Station, TX (Ocean Drilling Program).

Sinton, J.M., and Detrick, R.S., 1992. Mid-ocean ridge magma chambers. *J. Geophys. Res.,* 97:197–216.

Stakes, D., Mével, C., Cannat, M., and Chaput, T., 1991. Metamorphic stratigraphy of Hole 735B. *In* Von Herzen, R.P., Robinson, P.T., et al., *Proc. ODP, Sci. Results,* 118: College Station, TX (Ocean Drilling Program), 153–180.

Stakes, D.S., 1991. Oxygen and hydrogen isotope compositions of oceanic plutonic rocks: high-temperature deformation and metamorphism of oceanic layer 3. *In* Taylor, H.P., Jr., O'Neil, J.R., and Kaplan, I.R. (Eds.), *Stable Isotope Geochemistry: A Tribute to Samuel Epstein.* Spec. Publ. Geochem. Soc., 3:77–90.

Swift, S.A., Hoskins, H., and Stephen, R.A., 1991. Seismic stratigraphy in a transverse ridge, Atlantis II Fracture Zone. *In* Von Herzen, R.P., Robinson, P.T., et al., *Proc. ODP, Sci. Results,* 118: College Station, TX (Ocean Drilling Program), 219–226.

Thompson, G., and Melson, W.G., 1972. The petrology of oceanic crust across fracture zones in the Atlantic Ocean: evidence of a new kind of sea-floor spreading. *J. Geol.,* 80:526–538.

Tucholke, B.E., and Lin, J., 1994. A geological model for the structure of ridge segments in slow-spreading ocean crust. *J. Geophys. Res.,* 99:11937–11958.

Vanko, D.A., and Stakes, D.S., 1991. Fluids in oceanic layer 3: evidence from veined rocks, Hole 735B, Southwest Indian Ridge. *In* Von Herzen, R.P., Robinson, P.T., et al., *Proc. ODP, Sci. Results,* 118: College Station, TX (Ocean Drilling Program), 181–215.

Whitehead, J.A., Dick, H.J.B., and Shouten, H., 1984. A mechanism for magmatic accretion under spreading centers. *Nature,* 312:146–148.

APPENDIX

Because the hard-rock application of JANUS was not yet complete, and the old database (HARVI) had been discontinued, igneous data collected during this leg are recorded in a set of linked Microsoft Excel spreadsheets. Included on the CD-ROM are five linked spreadsheets (I_LITH.XLS, I_TEX.XLS, I_MIN.XLS, I_COMM.XLS, and DEPTHS.XLS), which cover lithologies, mineralogies, textures, and comments, and 20 independent spreadsheets, which cover coring, curation, metamorphic petrology, and structural geology. Listed below are the spreadsheet path names and the major column headers as they appear in each spreadsheet. These should be used as a guide to the spreadsheet contents. To open the spreadsheets, either click on the filenames in the right column or open the files through the Microsoft Excel application. To use the links, your computer must be configured to automatically launch Microsoft Excel when files with .XLS extensions are opened.

Igneous Spreadsheets

\176_IR\SUPP_MAT\APPENDIX\IGNEOUS\I_LITH.XLS

I_LITH.XLS

Lithology and Contact Reference Log

Lithol. Unit
Leg-Hole
Lower contact
  Core
  Sec.
  depth cur.
  Piece
  Depth mbsf
  Unit Thickness
  Type
  Form
Rock Type
  Grain size
  Modifier
  Rock name
  Special modifier
  Curated depth
  Curated thickness

\176_IR\SUPP_MAT\APPENDIX\IGNEOUS\I_TEX.XLS

I_TEX.XLS

Mineral Textures Log

Lithol. Unit
Leg-Hole
Lower contact
  Core
  Sec.
  depth cur.
  Piece
  Depth mbsf
Mineral shape
  plag.

aug.
oliv.
opx/pig.
opaq.
sulf.
Mineral habit
plag.
aug.
oliv.
opx/pig.
opaq.
sulf.
Mineral Color
Augite

\176_IR\SUPP_MAT\APPENDIX\IGNEOUS\I_MIN.XLS I_MIN.XLS

Mineralogy Log: Mode and Grain Size

Unit
Leg-Hole
Core
Sect.
Depth CDS
Piece
Depth mbsf
Mineralogy
Plagioclase (%, Max, Min, Ave)
Augite (%, Max, Min, Ave)
Olivine (%, Max, Min, Ave)
Opx/Pig (%, Max, Min, Ave)
Opaques (%)
Sulfides (%)
Unidentified (%)
Total
Grain size
weighted avg.
Diff.
fr 100
M
Grain Size
IUGS Rock Name

\176_IR\SUPP_MAT\APPENDIX\IGNEOUS\I_COMM.XLS I_COMM.XLS

Rock Fabric and Comment Log

Interval
Leg-Hole
Lower contact
Core
Sec.
depth cur.
Piece
Depth mbsf
width

Fabrics
type
dist
Structures
type
dist
Layers
Comments

\176_IR\SUPP_MAT\APPENDIX\DPTHSMTH\EXCOM\DEPTHS.XLS DEPTHS.XLS

(Hole 735B Depth Log)

Core
Length
Top Depth
Section curated length
0
1.00
2.00
3.00
4.00
5.00
6.00
7.00
8.00
Total
Recovery
Number of Sections

\176_IR\SUPP_MAT\APPENDIX\IGNEOUS\I_OPAQUE.XLS I_OPAQUE.XLS

Oxide Log

Unit
core
core #
section
Bottom contact
opaque
mbsl @ bottom

\176_IR\SUPP_MAT\APPENDIX\IGNEOUS\I_VEIN.XLS I_VEIN.XLS

Igneous Vein Log

Depth Interval (Per 10 meters)
Number of Vein or veinlets (Per 10 meters)
Volume % (Per 10 meters)

\176_IR\SUPP_MAT\APPENDIX\IGNEOUS\176GEOCH.XLS 176GEOCH.XLS

XRF and Thin-Section Log

Core

Type
SC
Top
Bot
RType
Code
Sam_ID
SiO2
TiO2
Al2O3
Fe2O3
MnO
MgO
CaO
Na2O
K2O
P2O5
Total
LOI
Mg_No
Ca_No
V
Cr
Ni
Cu
Zn
Rb
Sr
Y
Zr
Nb
Number
XRF/TS
Thin Section Label
Slide Rock Name from Point Counting
Thin Sect. MBSF
Interval #
Interval Rock Name from Core Descriptions
Thin Section Modes
Plag
Oliv
Cpx
Opx
Opaques
Amph
Zircon
Apatite
Other
Total
Points
Comments

Coring Summary Spreadsheet

\176_IR\SUPP_MAT\APPENDIX\CORESUMM\CORESUM.XLS CORESUM.XLS

Complete Coring Summary

Curation Spreadsheets

\176_IR\SUPP_MAT\APPENDIX\CURATION\PIECELOG.XLS PIECELOG.XLS

Curatorial Date Sheet/Piece Length

Core
Section
Pieces
Top
Bottom
Length
  Total length
  Liner length
  ll/tl
  Section depth top
  Section depth bottom

\176_IR\SUPP_MAT\APPENDIX\CURATION\SECTNLOG.XLS SECTNLOG.XLS

Curatorial Data Sheet/Section Depth

Core
Section
Piece
Top
Bottom
Core top depth
Section top depth
Section bottom depth

\176_IR\SUPP_MAT\APPENDIX\TS_LOG.XLS TS_LOG.XLS

Thin-Section Log

Leg-Hole
Core-Section
Interval (cm)
Piece
TS#

Metamorphic Petrology Spreadsheets

\176_IR\SUPP_MAT\APPENDIX\METAMORPH\BGALTLOG.XLS BGALTLOG.XLS

Hole 735B Alteration Log

Leg
Hole #

Core #
Section #
Piece #
Depth to Top of Piece (cm)
Piece Length (cm)
Extended Depth
Total Rock Alt (cm)
Alteration After Olivine
  Talc
  Amph
  Chl
  Smt
  Hmt
  Pyr
  Tot Olv Alt (%)
Alteration After Clinopyroxene
  Hbl
  Act
  Chl/ Smt
  Oxide
  Tot Cpx Alt (%)
Alteration After Plagioclase
  2nd Plg
  Zeolite
  Preh
  Chl/ Smt
  Tot Plg Alt (%)
Comments

\176_IR\SUPP_MAT\APPENDIX\METAMORPH\VEINLOG.XLS VEINLOG.XLS

Vein Log

Hole
Core
Section
Piece
Vein #
T
B
Length (cm)
Width (mm)
Depth (mbsf)
Area %
Area (cm2)
# of Veins per sec
Vein Type
Vein #
Amph
Plag
Cpx
Epi
Zois
Qtz
Chl
Oxi

Zeo
Sphene
Cc
Sm
Other
AW (cm)
%Alt
Minerals
Comments

\176_IR\SUPP_MAT\APPENDIX\METAMORPH\T_S_LOG.XLS T_S_LOG.XLS

Hole 735B Thin-Section Log

TS-#
Hole
Core
Section
Piece
Interval
Lith Unit
Rock Name
Total Rock Alt
Alteration After Olivine
- Talc
- Mt
- Amph
- Chl
- Smt
- Hmt
- Cc
- Pyr
- Tot Olv Alt

Alteration After Clinopyroxene
- Diop
- Hbl
- Act
- Chl/ Smt
- Oxide
- Tot Cpx Alt

Alteration After Orthopyroxene
- Amph
- Chl/ Smt
- Hem
- Tot Opx Alt

Alteration After Plagioclase
- 2nd Plg
- Epi
- Cc
- Oxide
- Other
- Chl/ Smt
- Act
- Tot Plg Alt

Comments

Vein Minerals
- Vein #
- Amph
- Plg
- Cpx
- Epi
- Qtz
- Chl
- Oxide
- Zeo
- Sph
- Cc
- Smt
- Other

Vein Halo
- AW
  - Alt
- Minerals

Comments

\176_IR\SUPP_MAT\APPENDIX\METAMORPH\VEIN%DEP.XLS

VEIN%DEP.XLS

Vein Percent of Recovered Core Log

Depth
Vein Percent Of Recovered Core Log
- Total vns
- Amph.
- Plag.
- pl+amp
- Diop.
- Pl+Di
- Felsic
- Carb.
- Chl.
- Smct.
- Zeolite
- Other

2 m running average percent
- Total vns
- Amph.
- Plag.
- pl+amp
- Diop.
- Pl+Di
- Felsic
- Carb.
- Chl.
- Smct.
- Zeolite
- Other

Structural Geology Spreadsheets

\176_IR\SUPP_MAT\APPENDIX\STRUCTUR\SPRDSHTS\FAULTS.XLS

FAULTS.XLS

- CURATORIAL DATA
  - Hole
  - Core
  - Section Number
  - Piece Number
  - Distance from top to top of the section (cm)
  - top depth (mbsl)
  - Distance from bottom to top of the section (cm)
  - bottom depth (mbsl)
- DEFORMATION INTENSITY
  - Breccias (B)
  - Faults (slip: n,r,d,s) (F)
  - Cataclastic Fabrics (Cf)
  - Thickness
- ORIENTATION
  - PLANES
    - Orientation on Working Half Face
    - dip 1, dir.1
    - 2nd apparent orientation or strike on horizontal plane
    - dip 2, dir.2
    - pole of the plane (core ref. frame)
    - dir., dip
    - strike and dip (core ref. frame)
    - strike, dip
    - strike and dip (geographic ref. frame)
    - strike, dip
  - LINES
    - pitch
    - orientation in the core reference frame
    - trend, plun.
    - geographic orientation
    - trend, plun.
- COMMENTS

\176_IR\SUPP_MAT\APPENDIX\STRUCTUR\SPRDSHTS\INTENSTY.XLS

INTENSTY.XLS

- shm intensity
- interval
- BxC
- SUM (D)
- SUM (C)
- final averaged intensity
- depth

\176_IR\SUPP_MAT\APPENDIX\STRUCTUR\SPRDSHTS\MAGMATIC.XLS

MAGMATIC.XLS

- CURATORIAL DATA
  - Hole

Core
Section Number
Piece Number
Distance from top to top of the section (cm)
Distance from bottom to top of the section (cm)
Depth (m)
DEFORMATION INTENSITY
Magmatic Fabrics (Mf)
Compositional Layering (Cl)
Igneous Contacts (Ic)
Interval Thickness
ORIENTATION
PLANES
Orientation on Working Half Face
dip 1, dir.1
2nd apparent orientation or strike on horizontal plane
dip 2, dir.2
pole of the plane (core ref. frame)
dir., dip
strike and dip (core ref. frame)
strike, dip
strike and dip (geographic ref. frame)
strike, dip
LINES
pitch in the foliation plane
pitch
orientation in the core reference frame
trend, plun.
geographic orientation
trend, plun.
COMMENTS

\176_IR\SUPP_MAT\APPENDIX\STRUCTUR\SPRDSHTS\PLASTIC.XLS

PLASTIC.XLS

CURATORIAL DATA
Hole
Core
Section Number
Piece Number
Distance from top to top of the section (cm)
Distance from bottom to top of the section (cm)
DEFORMATION INTENSITY
Crystal-Plastic fabrics (Pf)
Sense of Shear on the working half
ORIENTATION
PLANES
Orientation on Working Half Face
dip 1, dir.1
2nd apparent orientation or strike on horizontal plane
dip 2, dir.2
pole of the plane (core ref. frame)
dir., dip
strike and dip (core ref. frame)
strike, dip
strike and dip (geographic ref. frame)

strike, dip
LINES
pitch in the foliation plane
pitch
orientation in the core reference frame
trend, plun.
geographic orientation
trend, plun.
COMMENTS

\176_IR\SUPP_MAT\APPENDIX\STRUCTUR\SPRDSHTS\STRUCLOG.XLS

STRUCLOG.XLS

Structure Log

CURATORIAL DATA
Hole
Core
Section Number
Piece Number
Distance from top to top of the section (cm)
Distance from bottom to top of the section (cm)
DEFORMATION INTENSITY
Breccias (B)
Faults (offset: n,r,d,s) (F)
Cataclastic Fabrics (Cf)
Thickness
ORIENTATION
PLANES
Orientation on Working Half Face
dip 1, dir.1
2nd apparent orientation or strike on horizontal plane
dip 2, dir.2
Measured orientation In the core reference frame
strike, dip
LINES
Pitch in the foliation plane
pitch
orientation in the core reference frame
trend, plun.
COMMENTS

\176_IR\SUPP_MAT\APPENDIX\STRUCTUR\SPRDSHTS\VEINDPTH.XLS

VEINDPTH.XLS

Vein Depth

Hole
Core
Section
Interval top / cm
Interval bottom / cm
Interval centre / cm
depth of interval base / mbsf
joint intensity
SHM intensity

Vein intensity
pole plunge
vein strike
vein dip / direction

\176_IR\SUPP_MAT\APPENDIX\STRUCTUR\SPRDSHTS\VEINS.XLS

VEINS.XLS

Veins

CURATORIAL DATA
- Hole
- Core
- Section Number
- Piece Number
- Distance from top to top of the section (cm)
- Distance from bottom to top of the section (cm)

DEFORMATION INTENSITY
- Joints (J)
- Sub-horizontal microfractures (SHM)
- Veins (V)
- Cleavages/Folds (C/F)

(VEINS?)
- Number of Veins, joints, ...
- Vein type
- correlation with metam. vein log

ORIENTATION
- Orientation on Working Half Face
  - dip 1, dir.1
- 2nd apparent orientation or strike on horizontal plane
  - dip 2, dir.2
- pole of the plane (core ref. frame)
  - dir., dip
- strike and dip (core ref. frame)
  - strike, dip
- strike and dip (geographic ref. frame)
  - strike, dip
- Depth

COMMENTS

\176_IR\SUPP_MAT\APPENDIX\STRUCTUR\SPRDSHTS\XCUT.XLS

XCUT.XLS

Crosscutting Relationships

CURATORIAL DATA
- Hole
- Core
- Section Number
- Piece Number
- Distance from top to top of the section (cm)
- Distance from bottom to top of the section (cm)
- depth (mbsf) to top of the section (m)
- depth (mbsf) to bottom of the section (m)

ROCK NAME AND INTERVAL NUMBER
CROSS-CUTTING RELATIONSHIPS

COMMENTS

\176_IR\SUPP_MAT\APPENDIX\STRUCTUR\SPRDSHTS\CPFABRIC.XLS

CPFABRIC.XLS

Crystal-Plastic Fabrics

CURATORIAL DATA
- Hole
- Core
- Section Number
- Piece Number
- Distance from top to top of the section (cm)
- Distance from bottom to top of the section (cm)
- depth to top of interval (mbsf)
- depth to bottom of interval (mbsf)
- length of interval (m)
- length times Pf
- 11 cell sum of Length*Pf
- length of 11 cell sum
- running average of intensity
- 5 meter smooth
- 2.95 meter smooth

DEFORMATION INTENSITY
- Crystal-Plastic fabrics
- Sense of Shear on the workinf half

(ORIENTATION?)
- pole of the plane (core ref. frame)
  - dir., dip
- strike (core ref)
  - strike, dip
- (core ref. frame)
  - dip

Figure F1. Location of the Atlantis II Fracture Zone and Hole 735B. Position of the Southwest Indian Ridge, based on recent satellite gravity maps of the southern oceans and bathymetric data.

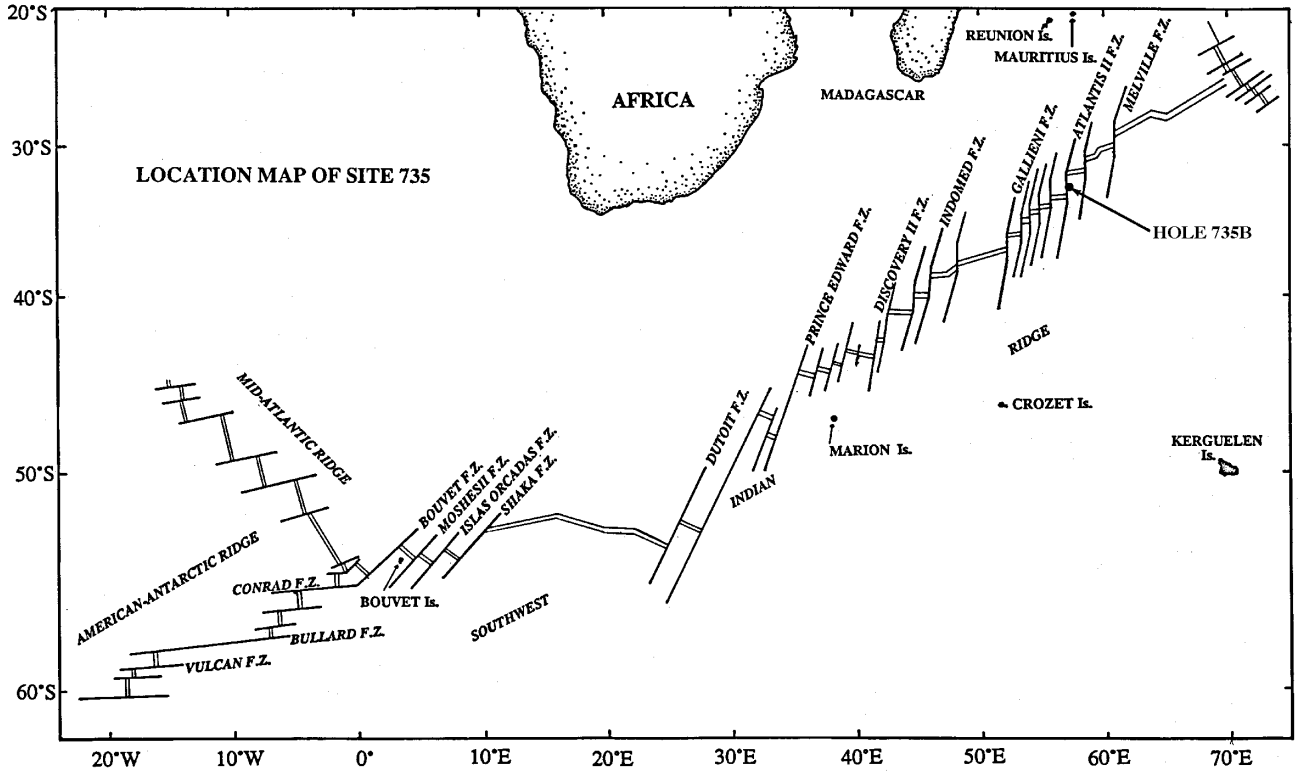

Figure F2. Bathymetric map of the Atlantis II Fracture Zone modified from Dick et al. (1991b). Locations of Hole 735B and the conjugate site 735B′ (SWIR 6) are shown. SWIR 6 is located on the counter lithospheric flow line on crust of the same age and position relative to the paleo-transform as Hole 735B. Note that the spreading rate is 1.0 cm/yr to the south and 0.6 cm/yr to the north. Active southern and northern rift valleys are at 33°40′S and 31°350′S, respectively.

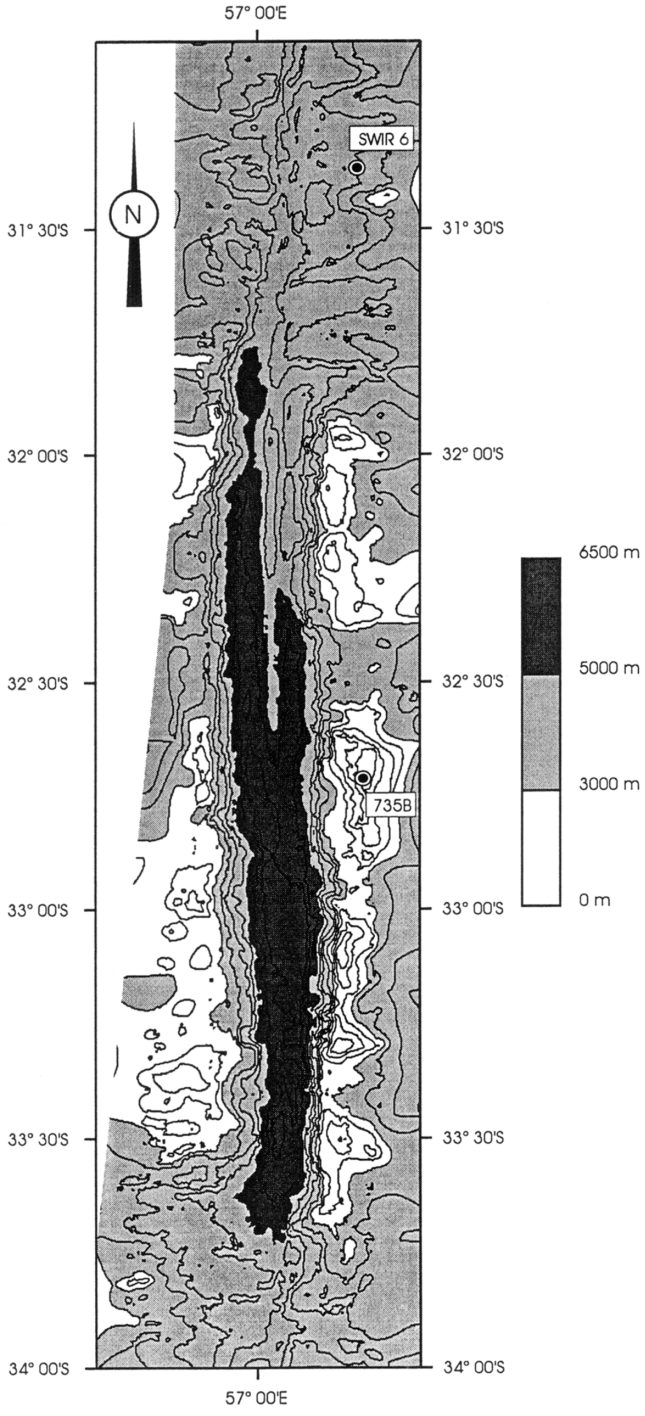

Figure F3. A. Hand-contoured 100-m-contour bathymetric map of Site 735 showing the location of Hole 735B, modified from Dick et al. (1991c). SeaBeam tracks were visually aligned to eliminate conflicts in transit satellite navigated data. The contour interval is 250 m. Small solid dots and arrows indicate the starting point and approximate track of dredge hauls. Large solid dots show the location of Sites 735 and 732 (just north of the contoured area on the crest of the median tectonic ridge). Solid circles indicate the approximate proportions of rock types recovered in each dredge: + = gabbro, white = basalt and diabase, light stipples = greenstone, and heavy stipples = serpentinized peridotite. **B.** Hand-contoured bathymetric map of the eastern rift mountains north of the Southwest Indian Ridge axis showing crust of the same age as that at Site 735 and the conjugate position of Hole 735B (735B′) on the counter-lithospheric flow line, based on magnetic anomalies and plate reconstruction. This conjugate site is the location of Southwest Indian Ridge 6, the proposed backup site for Leg 176, where the volcanic carapace originally overlying Hole 735B is preserved intact.

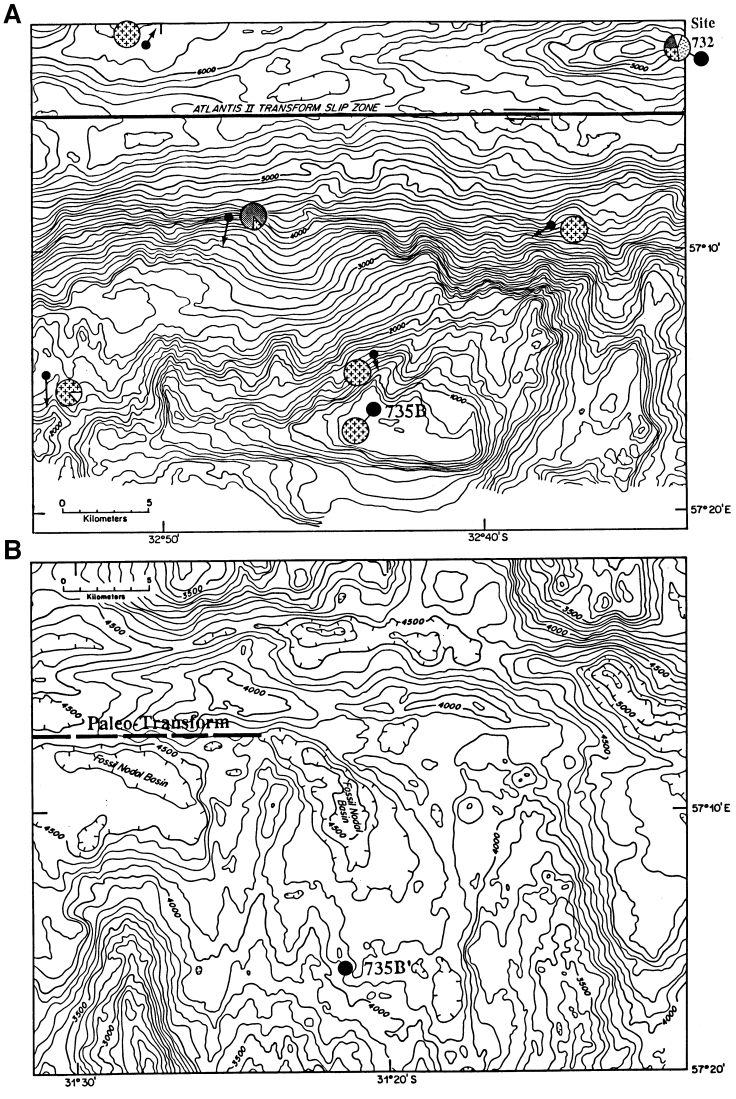

Figure F4. Magnetic anomalies over Site 735, based on the survey of Dick et al. (1991c) (M. Tivey, pers. comm. 1997). Bathymetry is contoured at 200-m intervals. Shading indicates crustal magnetization. Gray = normal-polarity crustal magnetization and white = reverse polarity. Dark gray areas have crustal magnetization >1 A/m. Polarity identifications and numbering modified from Dick et al. (1991c) by M. Tivey (pers. comm., 1997), based on the time scale of Cande and Kent (1995).

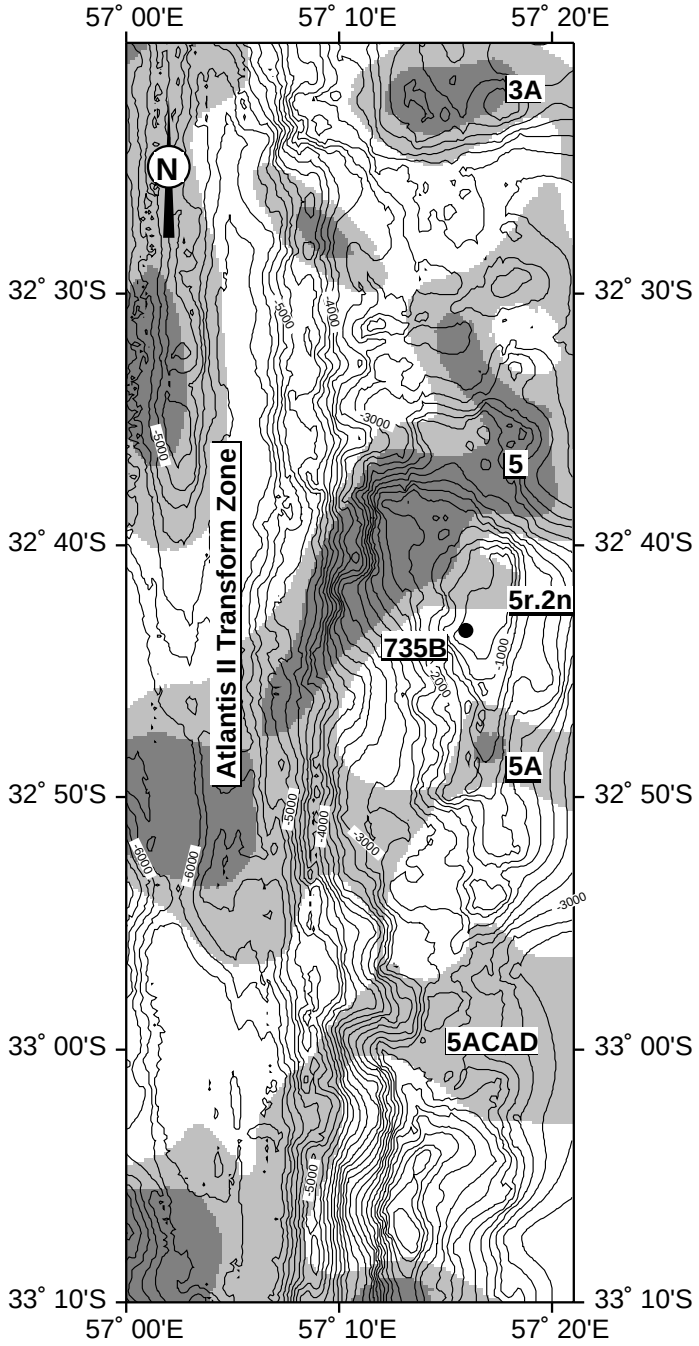

Figure F5. Outcrop map in the vicinity of Hole 735B constructed from a Leg 118 video survey. Video swath field of view = ~8 m. The ratio of outcrop to sediment is proportional to the distribution of patterns along the swath. Time stamp and depths from the video image and voice-over are noted along the swath pattern. Textured sediment refers to a coating of sediment so thin that the texture of the outcrop underneath is discernable. Locations of Holes 735A and 735B along the survey lines are also indicated.

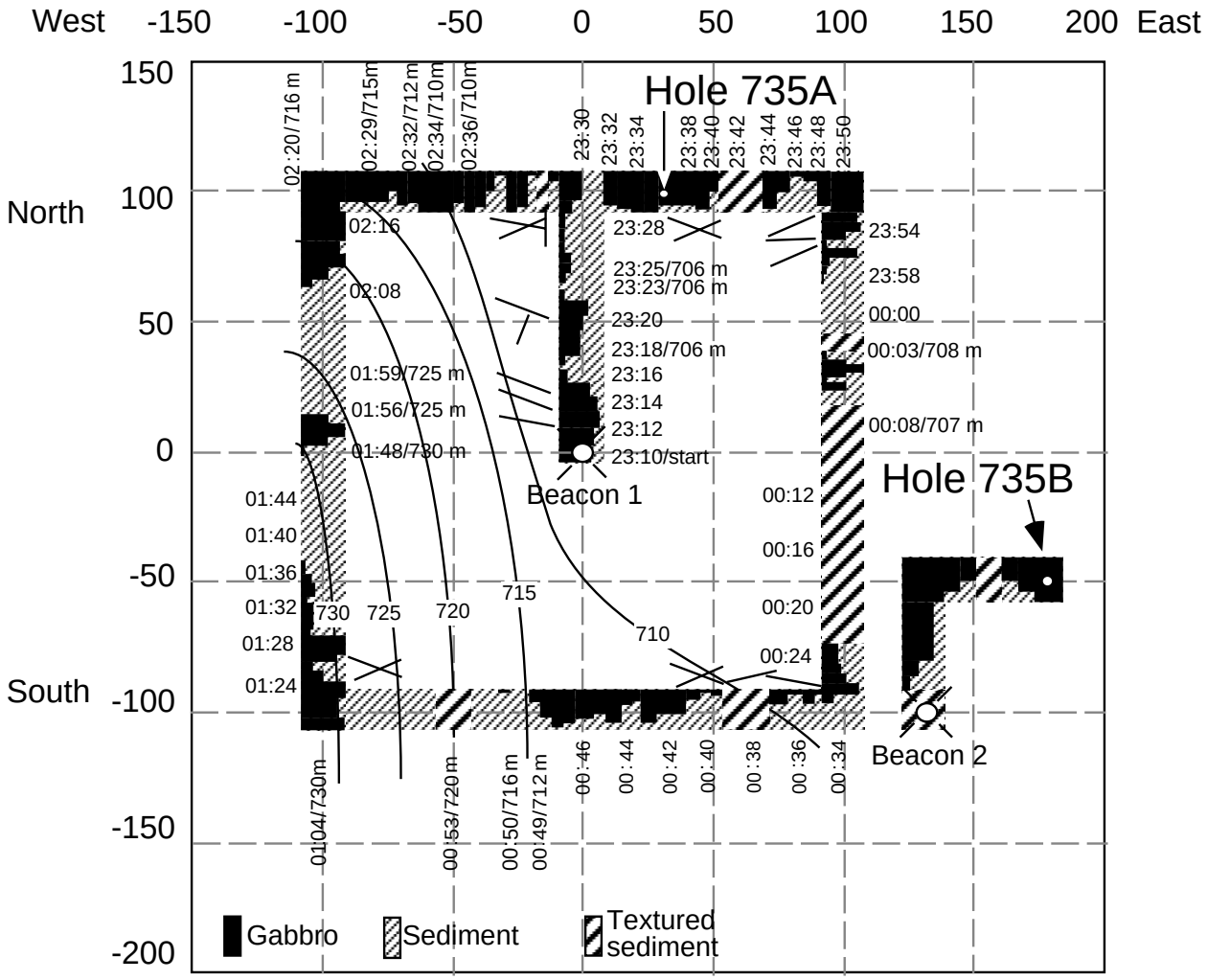

Figure F6. Temporal schematic cross sections across the Southwest Indian Ridge rift valley drawn parallel to the spreading direction (not across the fracture zone, but parallel to it), showing the postulated tectonic evolution of the transverse ridge and Hole 735B (Dick et al., 1991c). The sequential sections are drawn at about 18 km from the transform fault. Crust spreading to the right passes up into the transverse ridge and spreads parallel to the transform valley. Crust spreading to the left spreads into the rift mountains of the Southwest Indian Ridge parallel to the inactive extension of the Atlantis II Fracture Zone. **A.** Initial symmetric spreading, possibly at the end of a magmatic pulse. Late magmatic brittle-ductile deformation occurs because of lithospheric necking above (and in the vicinity of whatever passes for a magma chamber at these spreading rates). Hydrothermal alteration at high temperatures accompanies necking and ductile flow in subsolidus regions. **B.** At some point, the shallow crust is welded to the old, cold lithosphere to which the ridge axis abuts, causing formation of a detachment fault, and nodal basin, initiation of low-angle faulting, continued brittle-ductile faulting, and amphibolite-facies alteration of rocks drilled at Hole 735B. (Continued on next page.)

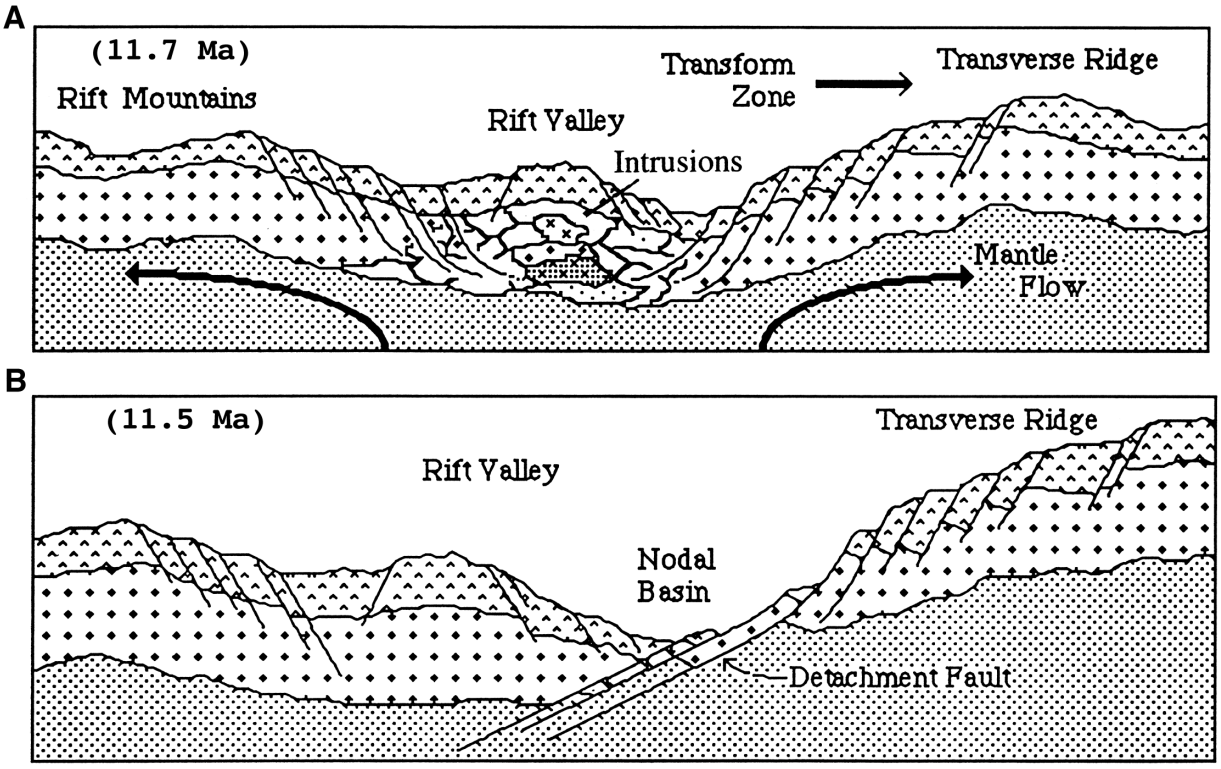

Figure F6 (continued). C, D. Block uplift of the rift mountains at the ridge-transform corner forms a transverse ridge. Initiation of the block uplift terminates the extension, driving excess cracking, and drastically reduces permeability in the Hole 735B rocks, effectively terminating most circulation of seawater and alteration. Greenschist-facies retrograde alteration continues along the faults on which the block is uplifted, accounting for the greenschist-facies alteration that predominates among dredged gabbros.

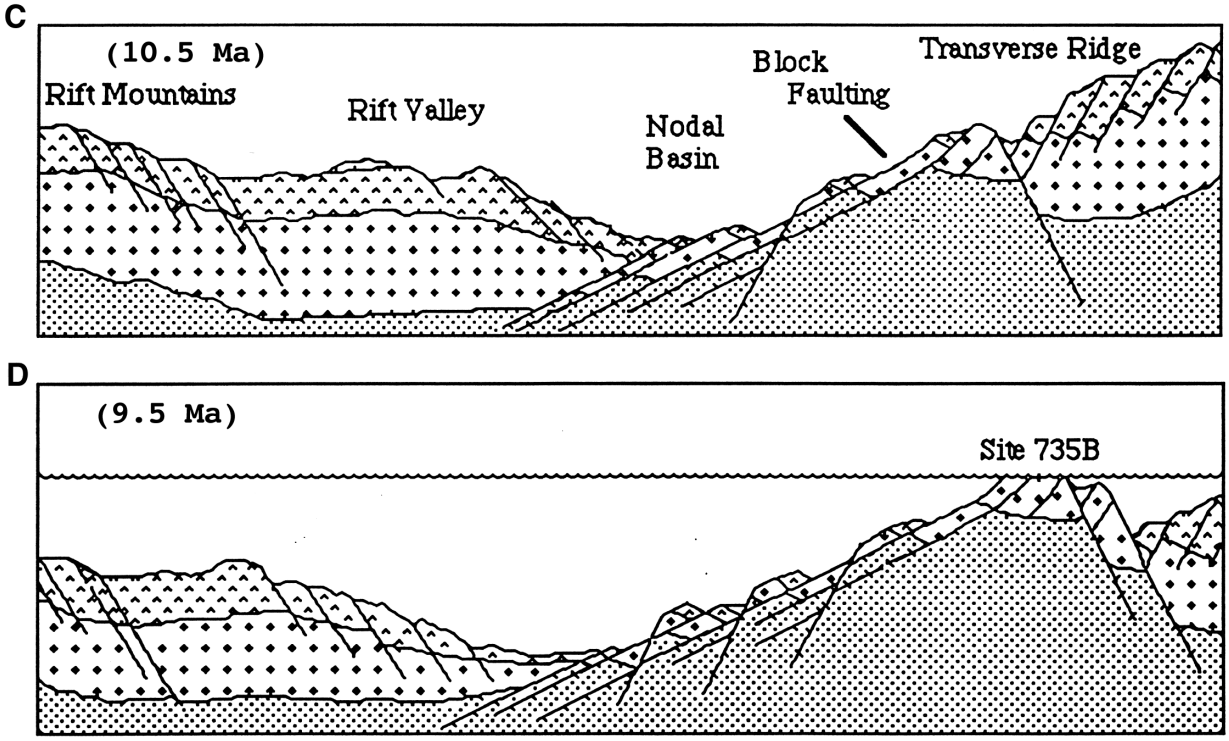

Figure F7. Seismic velocity structure from Muller et al. (1997). **A.** *P*-wave seismic velocity model on the north-south seismic Line CAM101 of Muller et al. (1997). The velocity contour interval is 0.3 km/s. Numbered OBS positions are shown on the seafloor. The position of ODP Hole 735B is projected from 1 km west of the line. The thicker line indicates Moho where its depth is constrained by wide-angle reflections. **B.** Resolution contours for the seismic model. The resolution of each velocity node is given by the diagonal of the inversion resolution matrix a number between 0.0 and 1.0, which is affected by the ray coverage sampling each node. Values of >0.5 are considered well resolved and reliable.

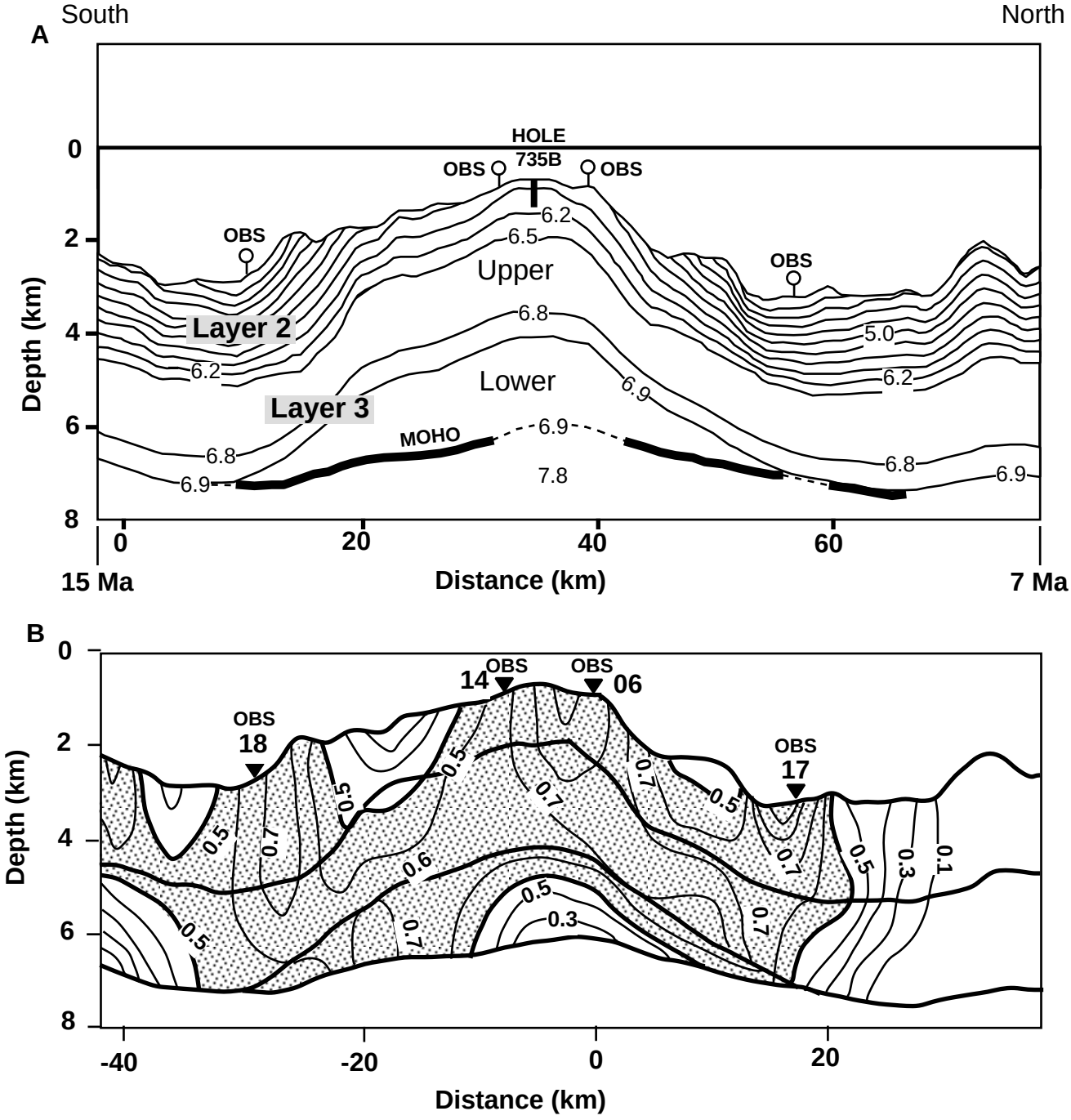

Figure F8. Lithostratigraphic column showing the change in proportions of igneous intervals through Hole 735B from the seafloor to 1508 mbsf and the locations of pegmatitic gabbros, microgabbros, and igneous layering. Plot represents a downhole running average of 20 igneous intervals. A total of 952 discrete igneous intervals were described and are included in the running average.

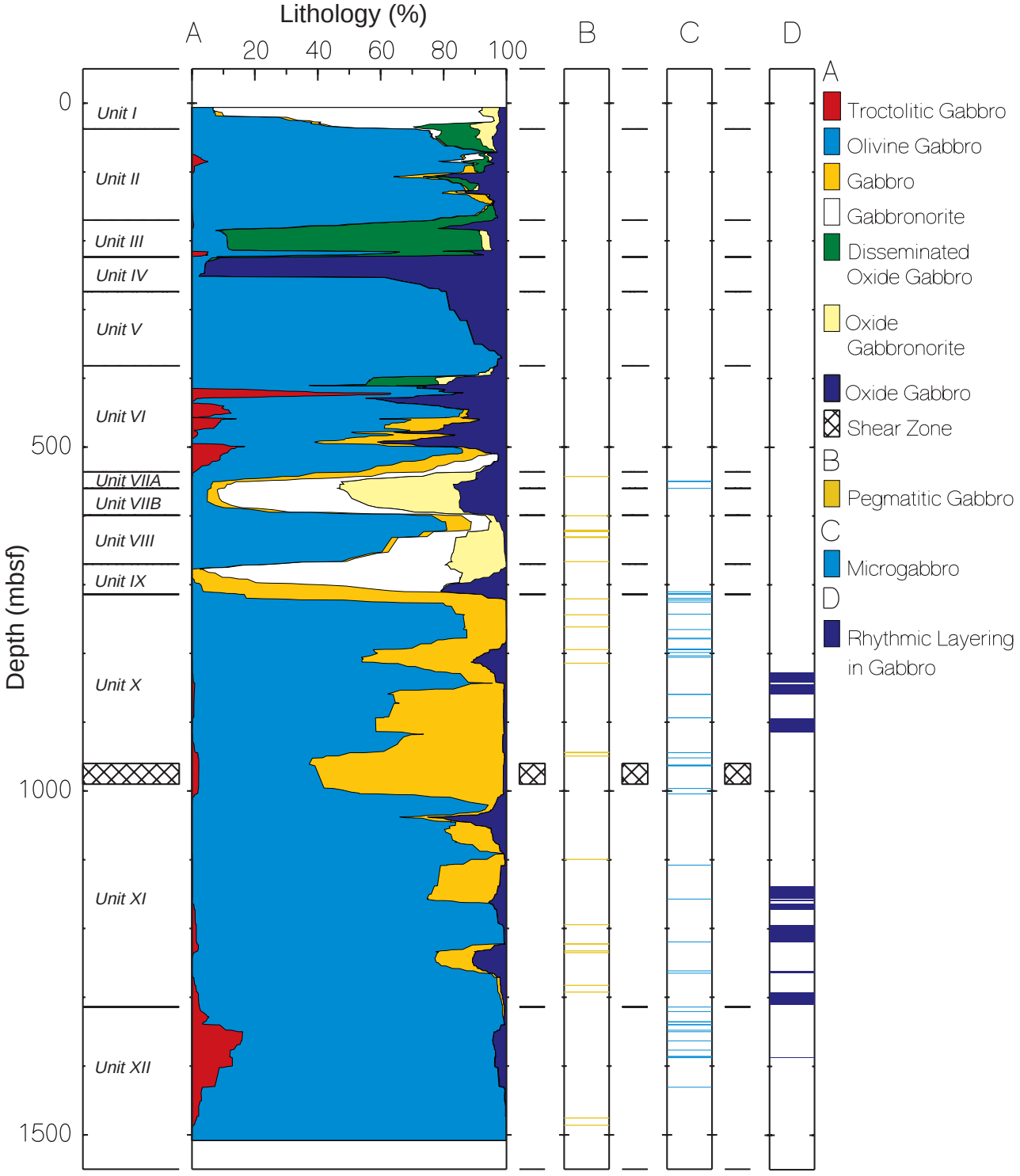

Figure F9. Representative close-up photographs of cores. **A.** Typical coarse-grained olivine gabbro (interval 176-735B-171R-2, 32–44 cm). **B.** Olivine microgabbro crosscutting olivine gabbro (interval 176-735B-189R-3, 90–120 cm). (Continued on next two pages.)

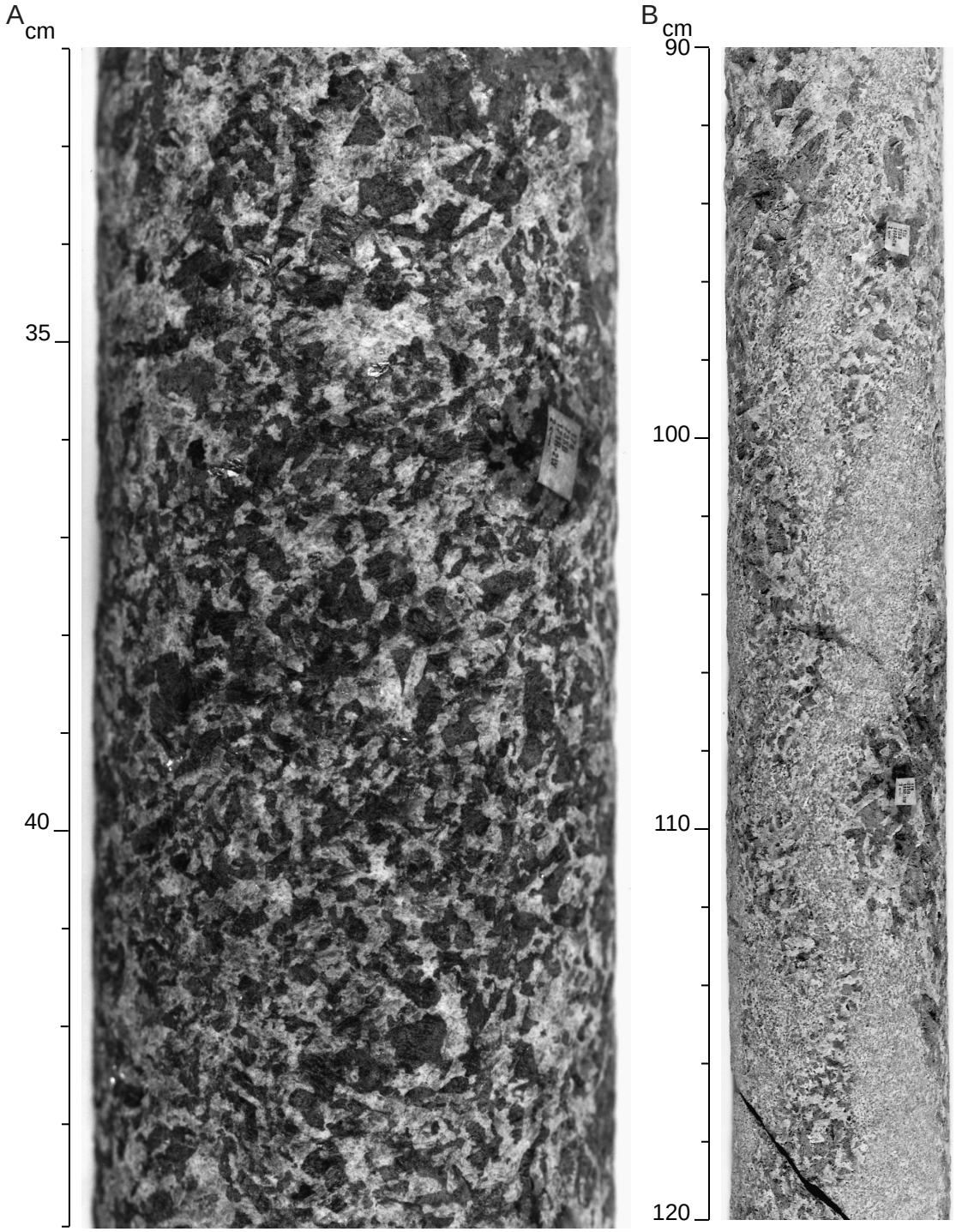

Figure F9 (continued). **C.** Oxide olivine gabbro vein crosscutting olivine gabbro (interval 176-735B-171R-2, 2–19 cm). **D.** Foliated gabbro (interval 176-735B-93R-3, 76–93 cm).

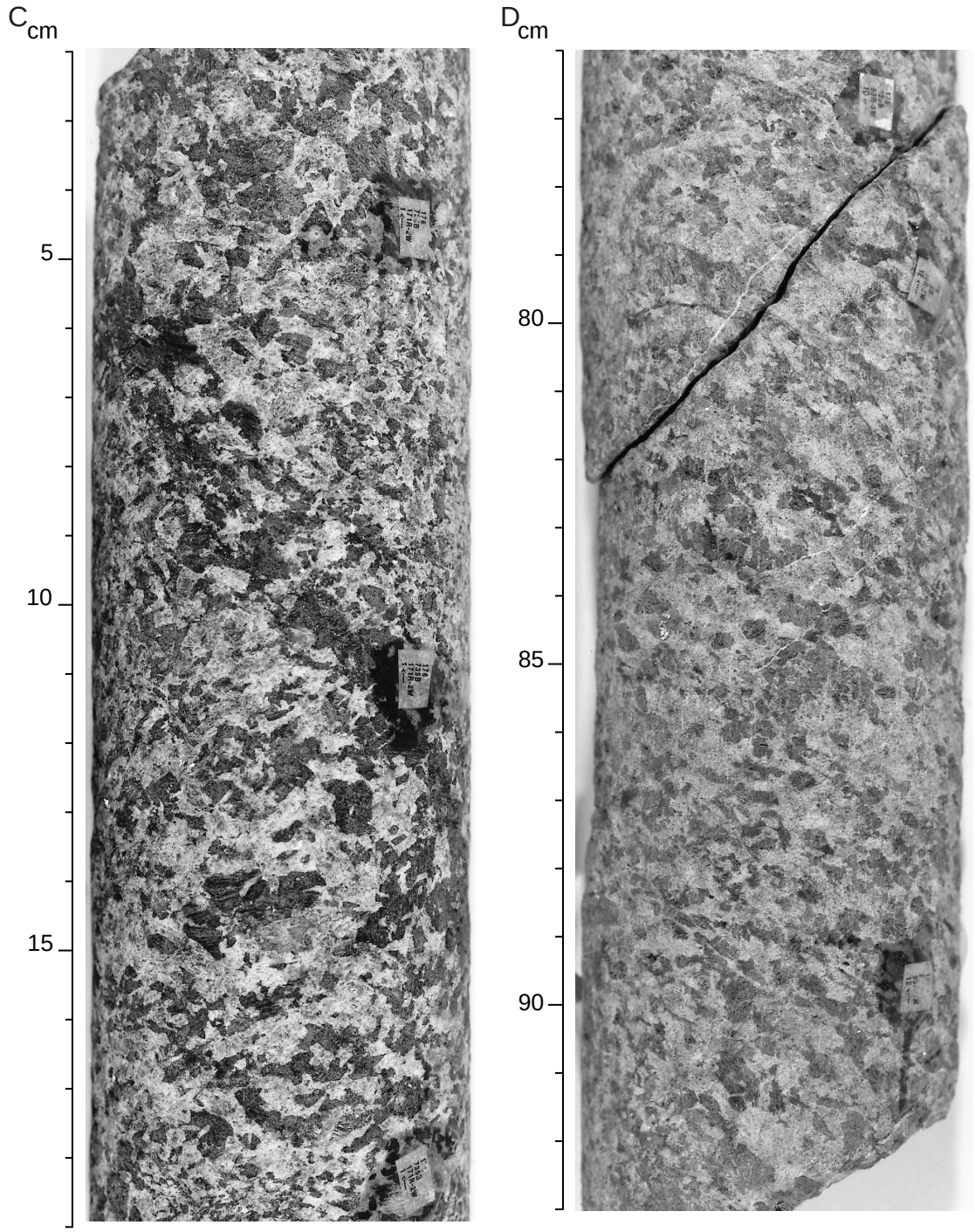

Figure F9 (continued). E. Pegmatoidal olivine gabbro (pieces from Sections 176-735B-177R-3 and 177R-4). **F.** Varitextured olivine gabbro (interval 176-735B-196R-5, 23–97 cm).

Figure F10. Representative layered sections of the Leg 176 core. **A.** Size-graded and modal layering (interval 176-735B-171R-4, 45–90 cm). **B.** Troctolitic layer in olivine gabbro (interval 176-735B-186R-4, 25–55 cm). **C.** Mafic layers in olivine gabbro (interval 176-735B-190R-2, 0–95 cm).

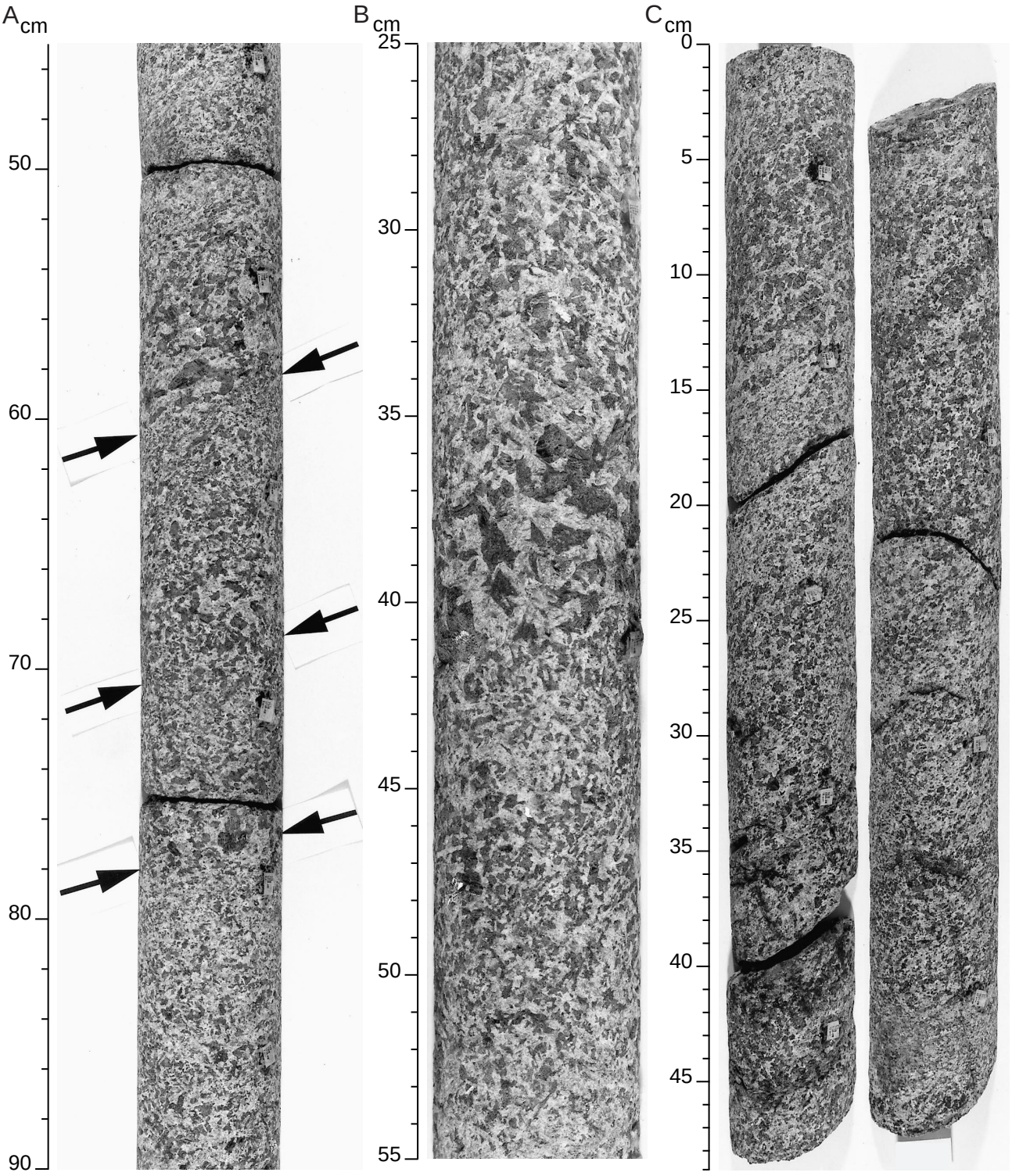

Figure F11. Downhole distribution of secondary phases in Hole 735B, related to the variation in total rock alteration with depth. Data are from thin-section observations.

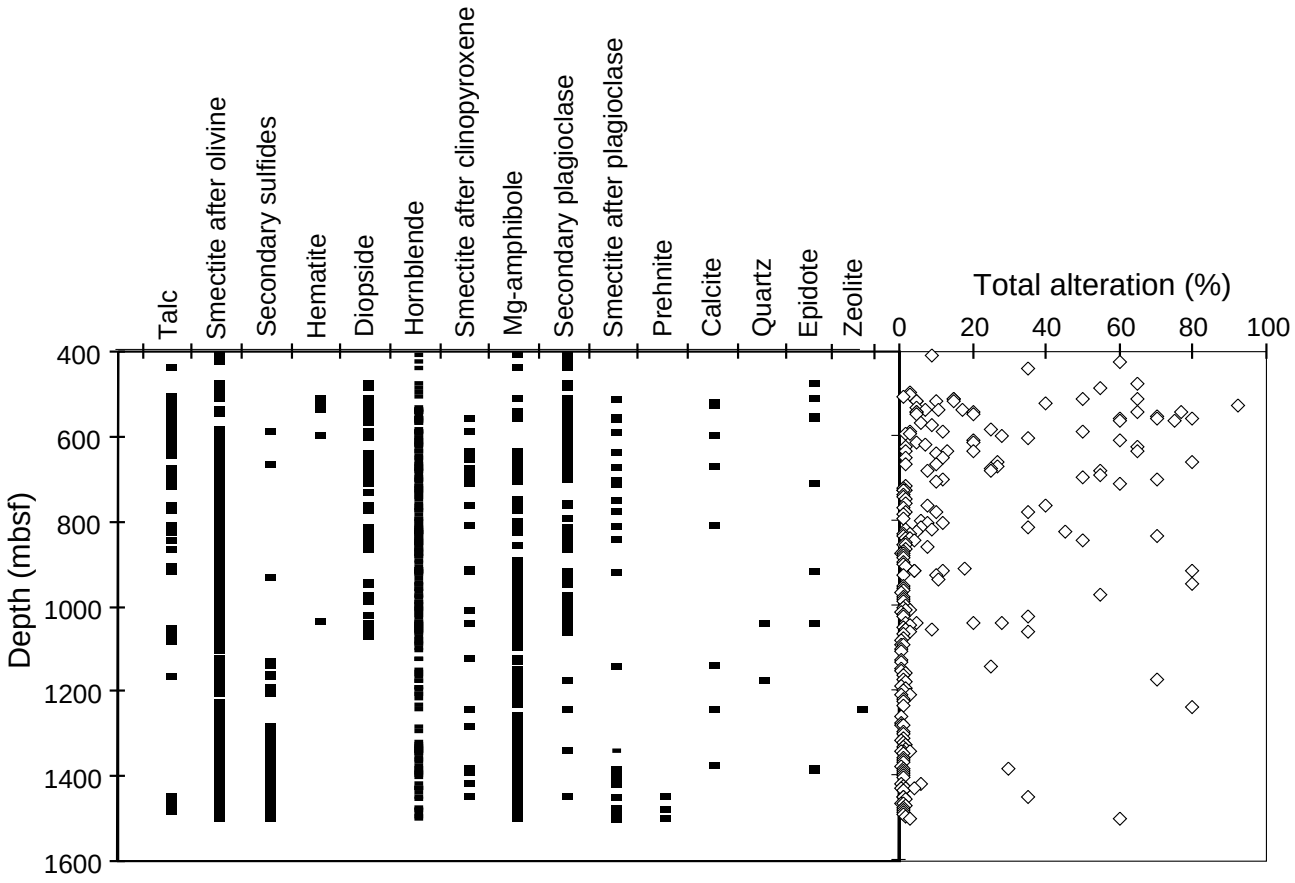

Figure F12. A. Percentage proportion of veins in cores of gabbroic rocks recovered during Legs 118 and 176. **B.** Distribution of felsic, plagioclase, and amphibole + plagioclase veins by percentage of core. Below 1250 mbsf, felsic veins are rare. **C.** Distribution of plagioclase + diopside and diopside veins by percentage of core. Below 750 mbsf, diopside and plagioclase + diopside veins are not present. **D.** Distribution of amphibole veins by percentage of core. Below 600 mbsf, amphibole veins are rare. **E.** Distribution of carbonate and smectite veins downsection. **F.** Distribution of chlorite and zeolite veins downsection.

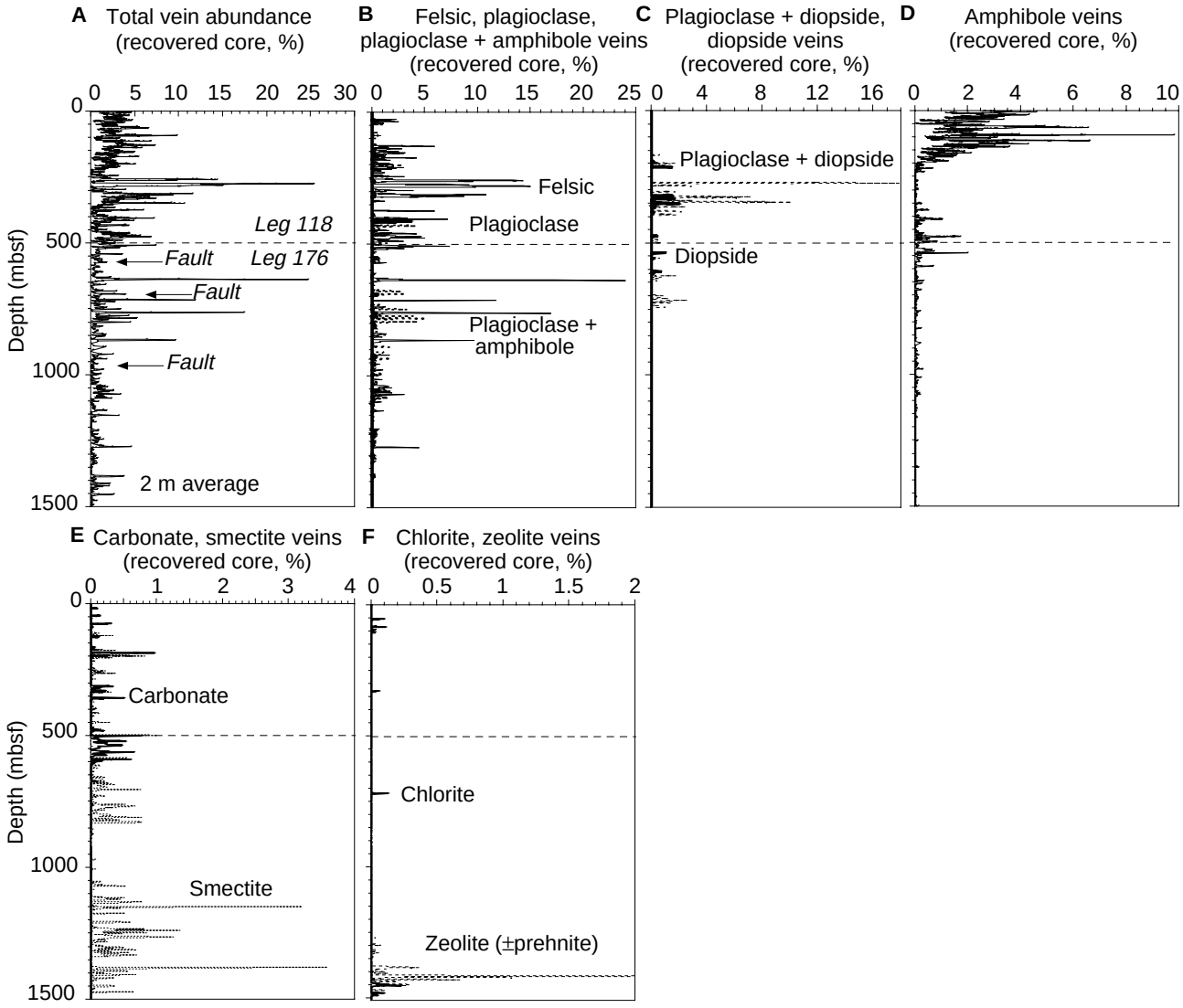

Figure F13. Plagioclase and diopside veins, and combinations thereof, on splays from an apparently igneous felsic vein (interval 176-735B-110R-4, 1–38 cm).

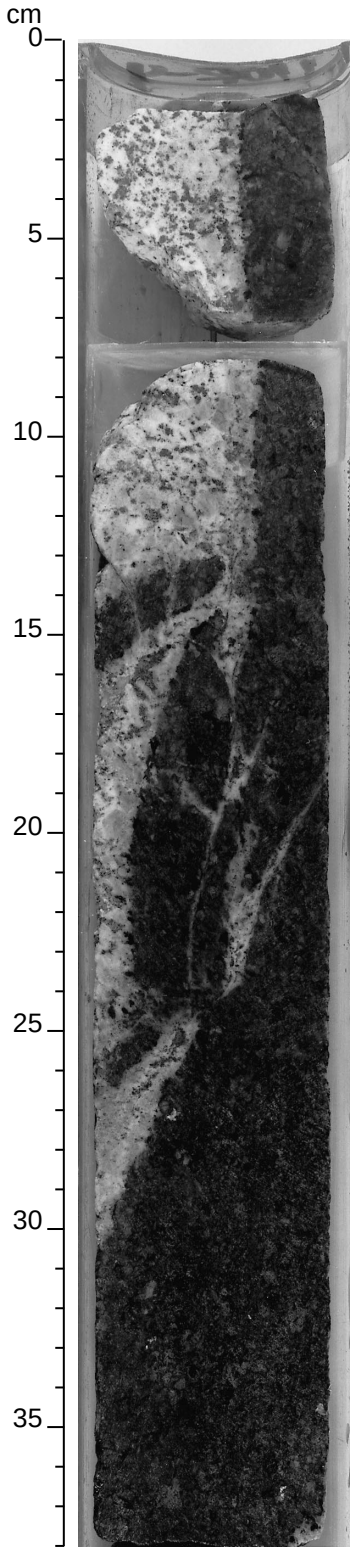

Figure F14. Subvertical amphibole vein crosscutting foliated olivine gabbro (interval 176-735B-92R- 1, 10–15 cm).

Figure F15. Vein of pale-green smectite in Sample 176-735B-133R-7 (Piece 1, 126–137 cm). Olivine, plagioclase, and clinopyroxene are highly altered to smectite in the alteration halo. Altered plagioclase appears pale green, altered olivine dark, and altered clinopyroxene brown or has a brilliant reflectance at greater distance from the vein (incipient alteration).

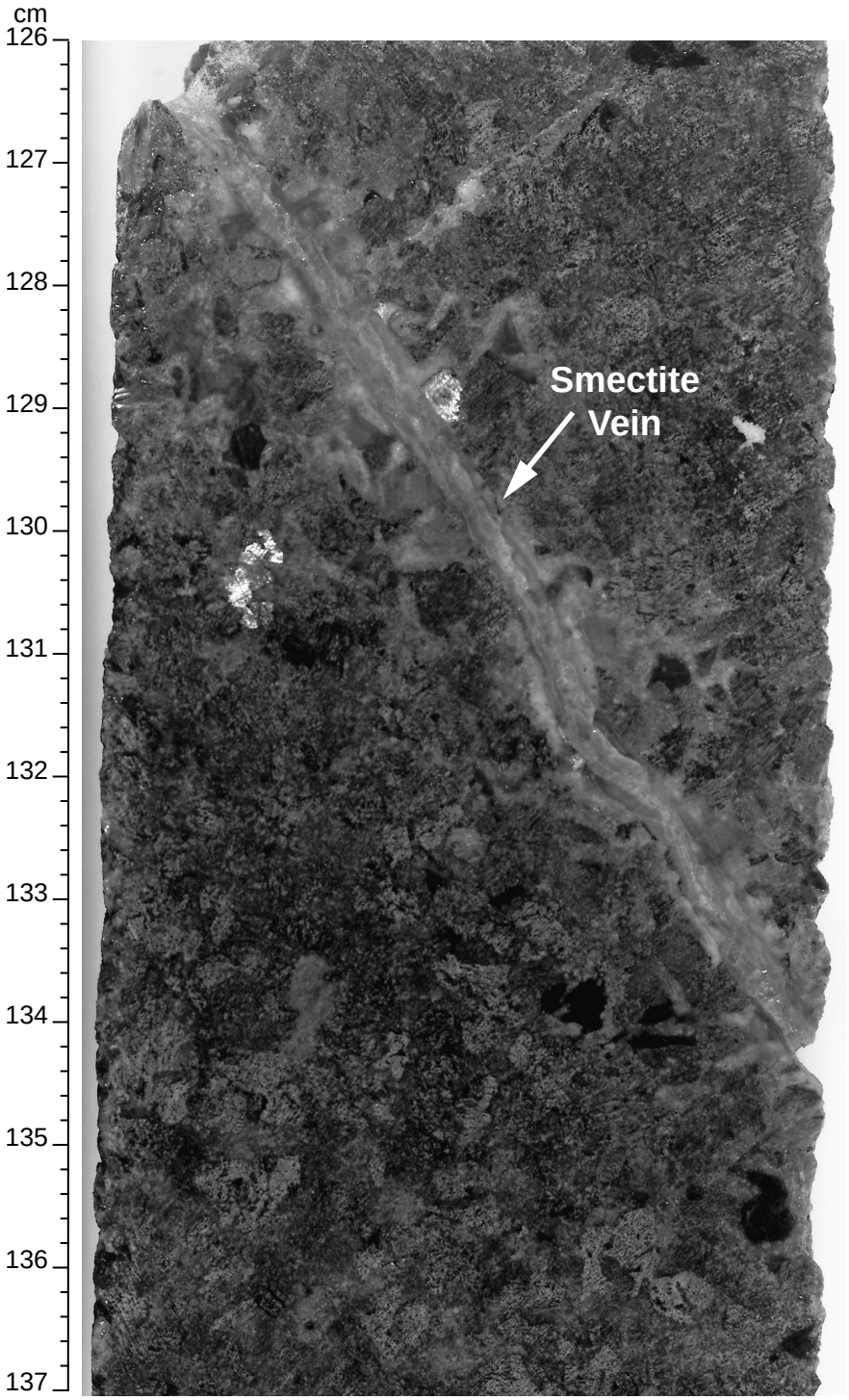

Figure F16. Mg# (calculated as $Mg^{2+}/Fe^{2+}+Mg^{2+}$; $Fe^{2+} = 0.85 \times Fe^{3+}$) vs. depth for Hole 735B. Gabbroic samples are subdivided on the basis of TiO_2 (see Fig. **F17,** p. 63). Filled diamonds = troctolite and olivine gabbro having less than 0.4 wt% TiO_2; half-filled diamonds = gabbro, gabbonorite, and disseminated-oxide gabbro having between 0.4 and 1.0 wt% TiO_2; open diamonds = Fe-Ti oxide gabbro with more than 1.0 wt% TiO_2; half-filled squares = felsic samples or hybrid samples with a significant felsic component. Filled triangle = a sample from a basaltic dike.

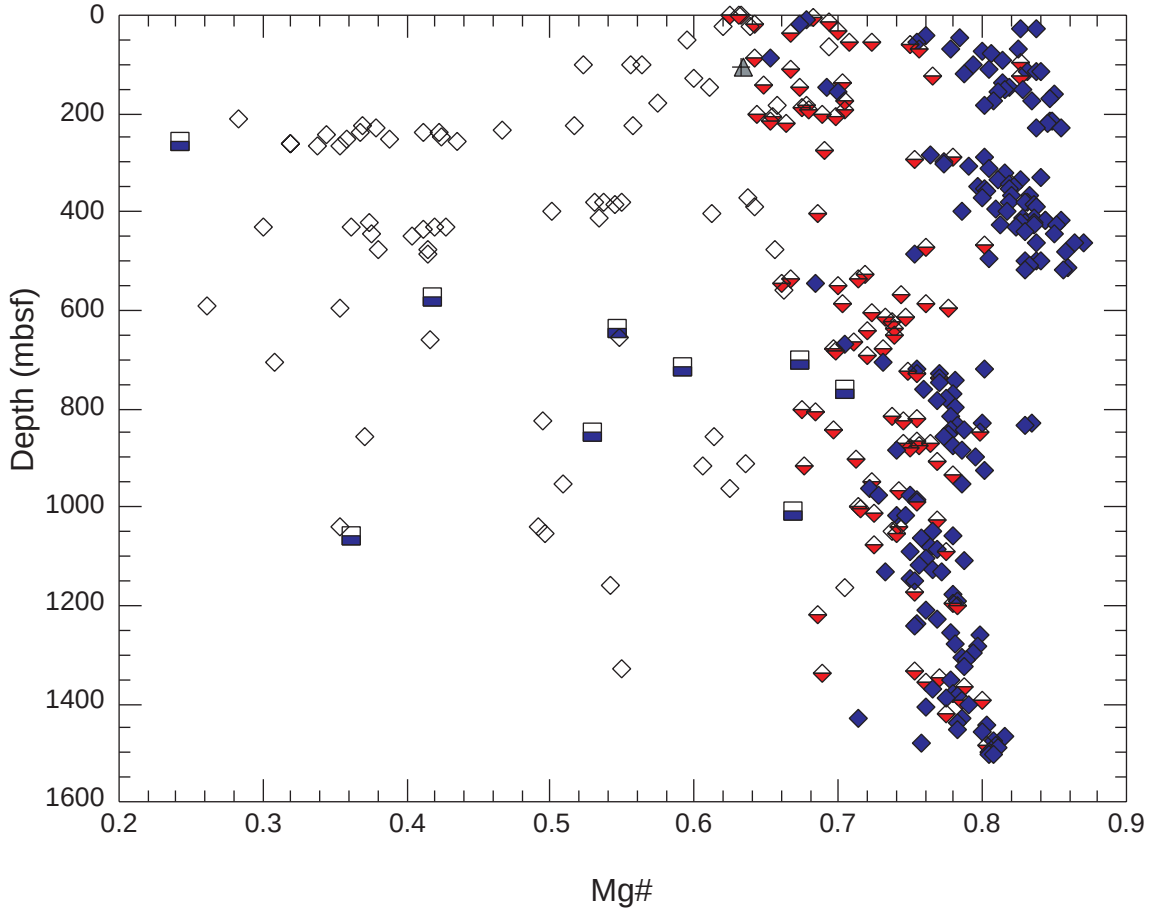

Figure F17. Log weight percent TiO_2 vs. depth in Hole 735B. Filled diamonds = troctolite and olivine gabbro having less than 0.4 wt% TiO_2; half-filled diamonds = gabbro, gabbonorite, and disseminated-oxide gabbro having between 0.4 and 1.0 wt% TiO_2; open diamonds = Fe-Ti oxide gabbro with more than 1.0 wt% TiO_2; half-filled squares = felsic samples or hybrid samples with a significant felsic component. Filled triangle = a sample from a basaltic dike.

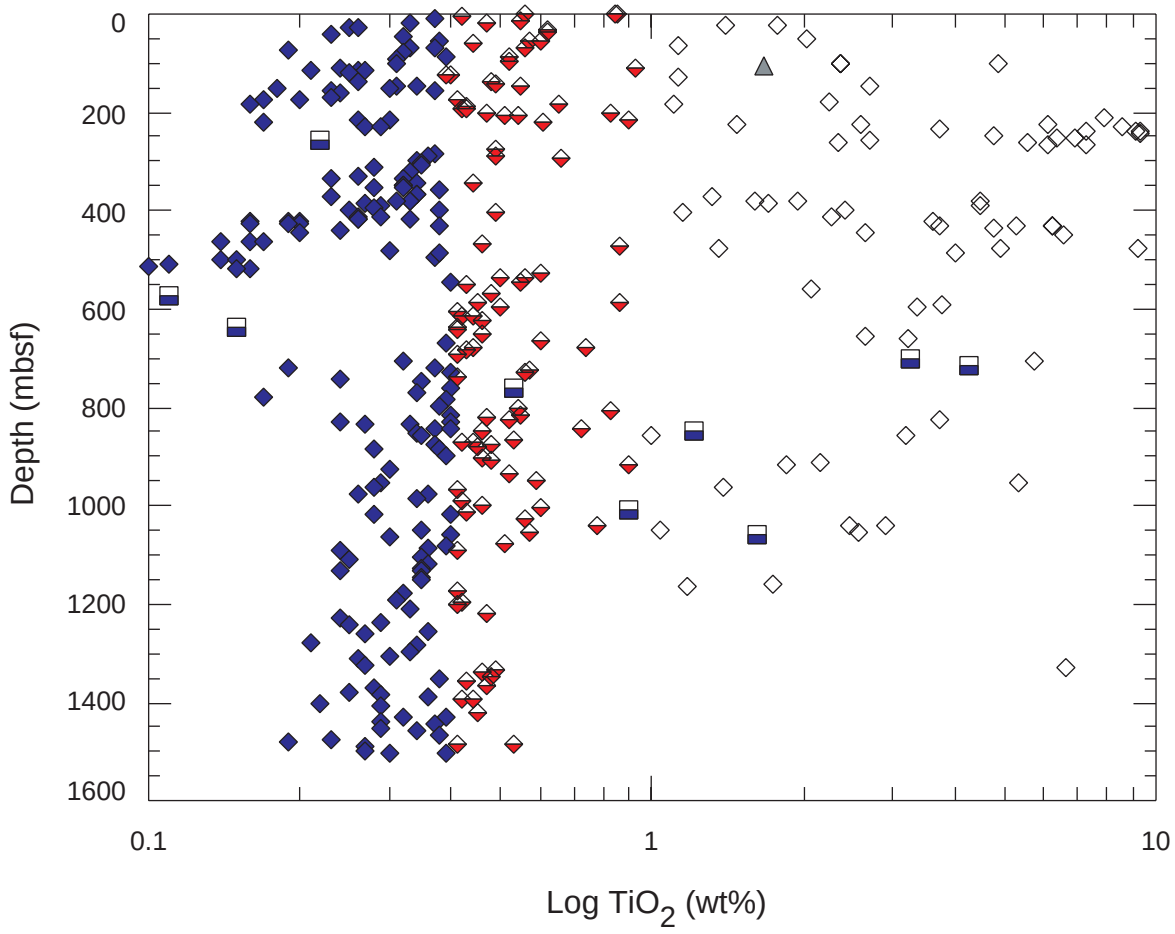

Figure F18. A. Late magmatic and crystal-plastic foliation intensities plotted with total vein intensities downhole for Hole 735B. No data on magmatic foliation exist for the upper 500 m of Hole 735B. (Continued on next page.)

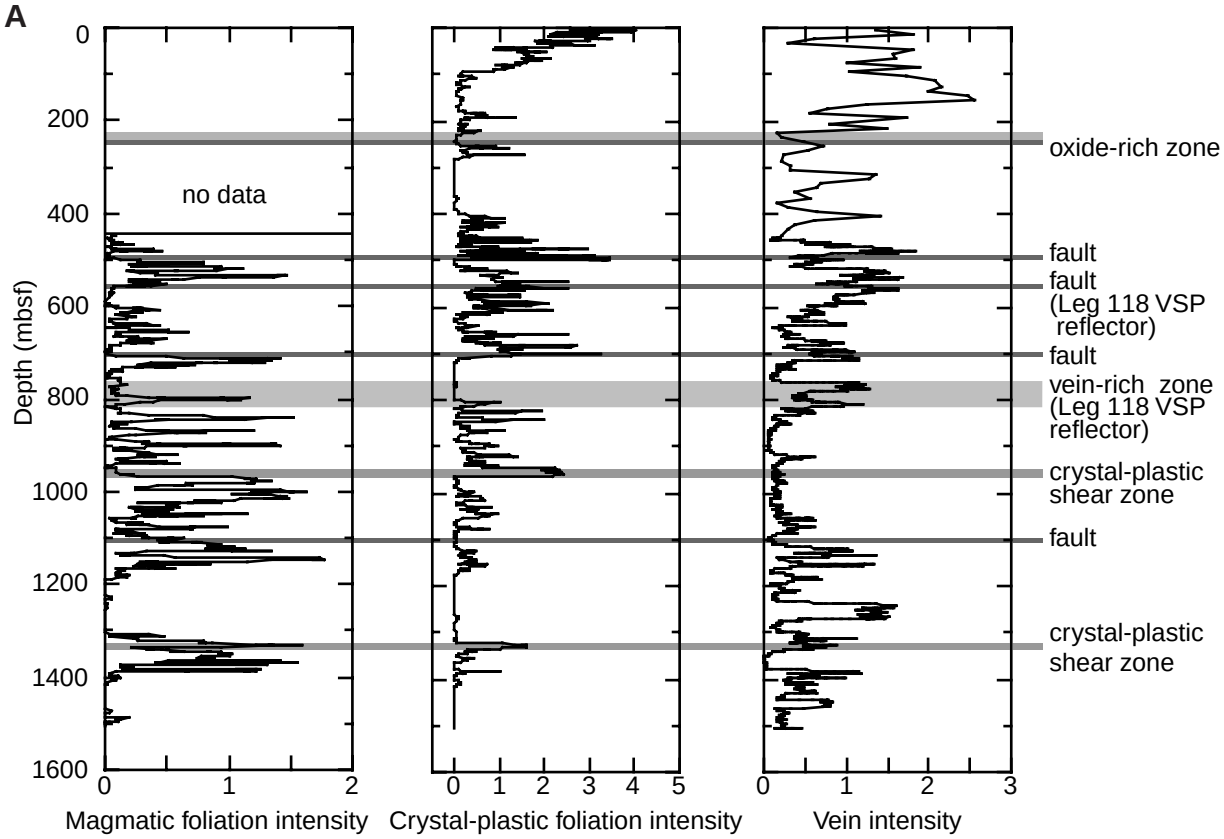

Figure F18 (continued). B. Stereoplots for structures in Hole 735B cores. Poles to foliation are plotted in the reference frame of the core liner, with the strong azimuthal orientation reflecting careful cutting of cores orthogonal to foliation and consistent placement in the core liners for description with respect to foliation dip. **C.** Representative photomicrographs of magmatic foliation, high-temperature (granulite grade) mylonite, and low-temperature cataclastic deformation.

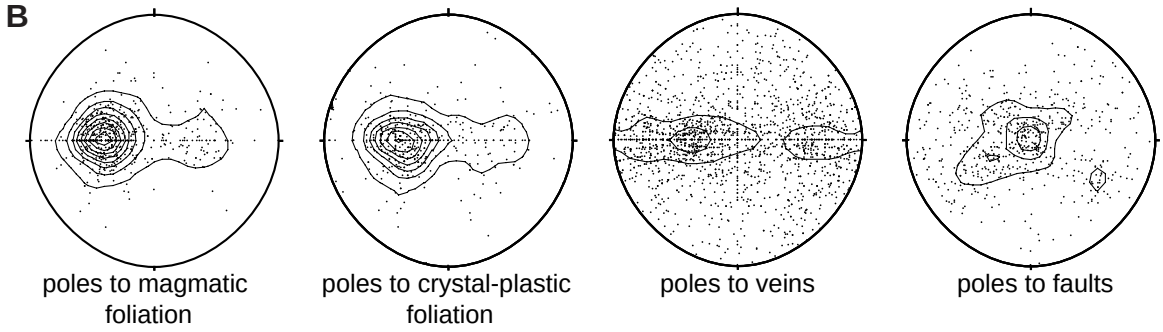

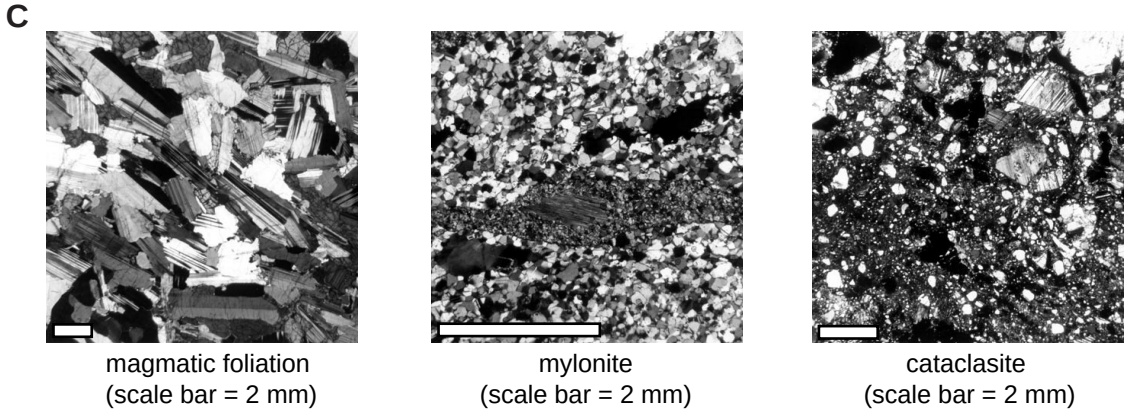

Figure F19. Close-up photograph of reverse fault (interval 176-735B-149R-3, 48–94 cm) at the base of a 20-m-thick shear zone. Note the abrupt transition to undeformed gabbro below 85 cm.

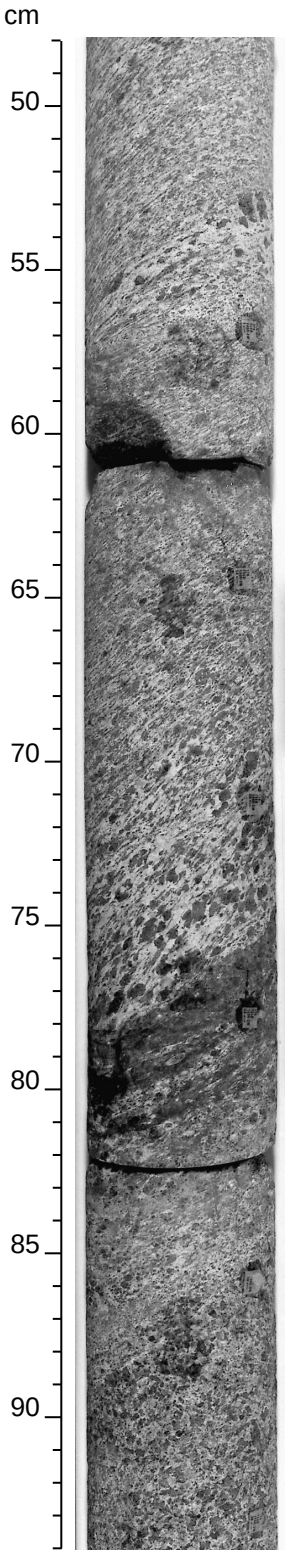

Figure F20. Stable thermal remanent magnetism, magnetic susceptibility, and inclination for Hole 735B after demagnetization of minicores.

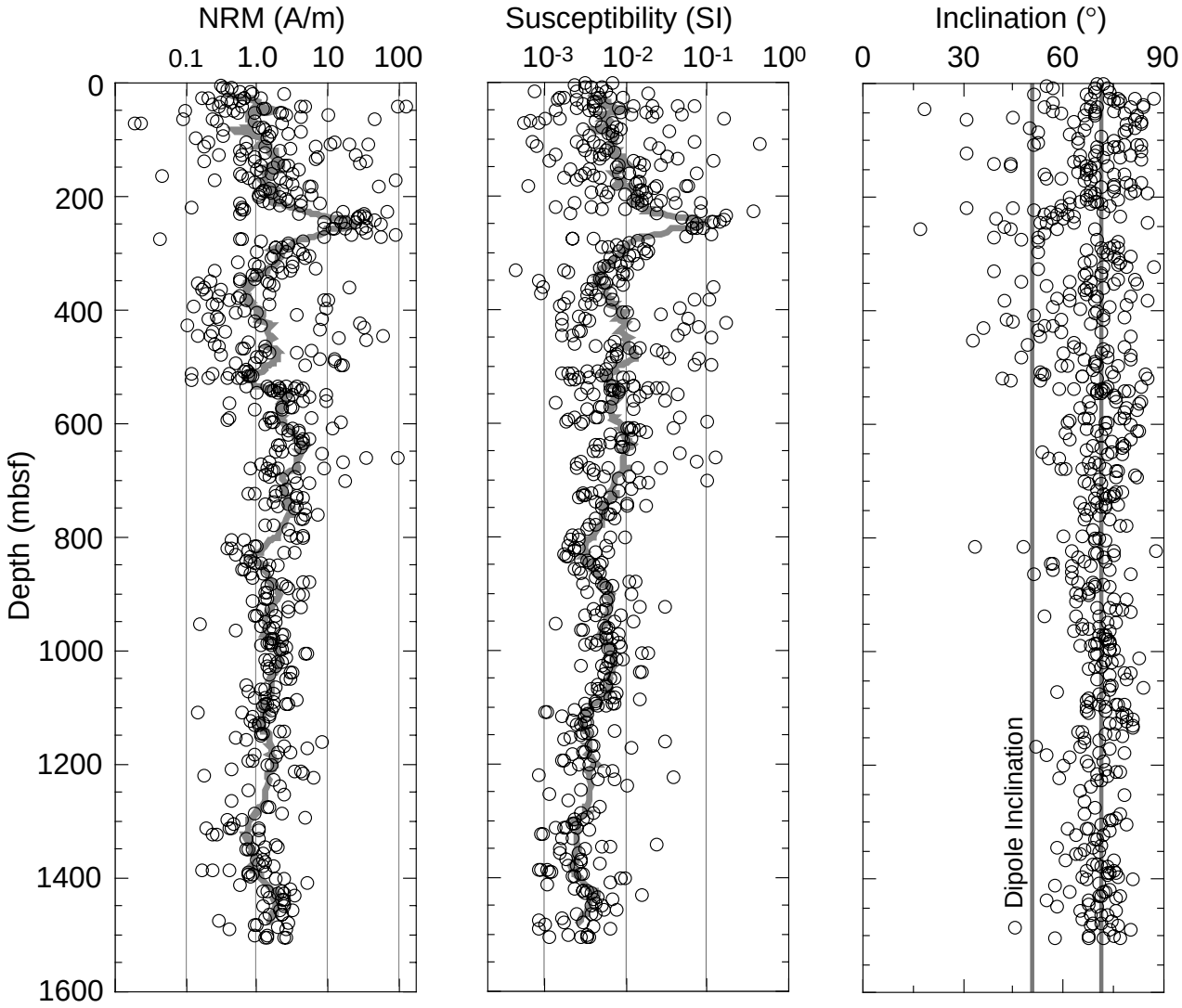

Figure F21. MST log of magnetic susceptibility for all cores from the Leg 176 section of Hole 735B. Measurements are filtered to eliminate empty sections of the core liners, leaving in excess of 22,000 measurement points. Inset shows correlations between individual peaks and lithologies in a section of core from 1072 to 1084 mbsf. LI = lithologic interval; OxG = oxide gabbro; FV = felsic vein; and OG = olivine gabbro.

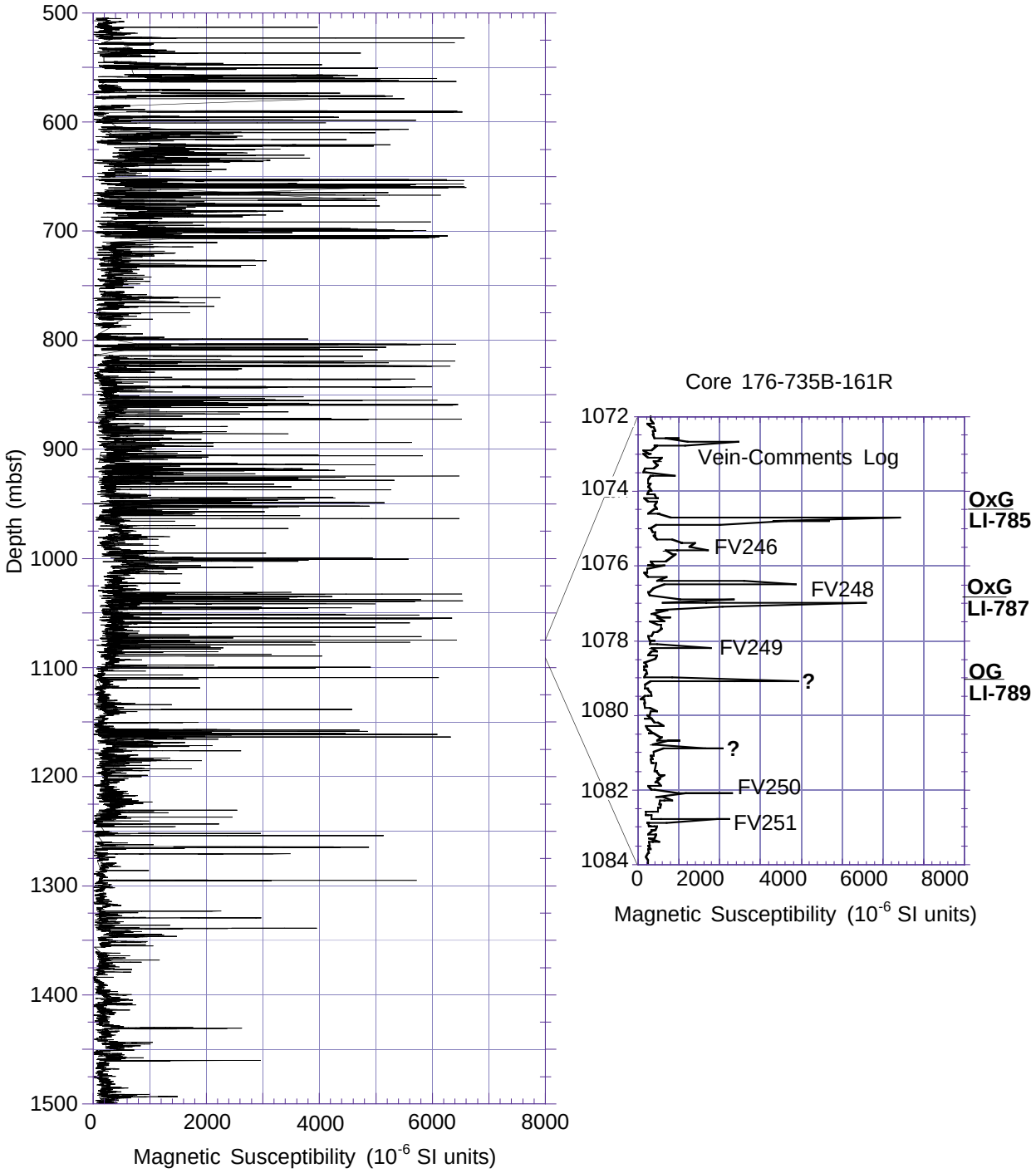

Figure F22. Comparison of discrete sample bulk density and velocity with percent recovery downhole. Dashed lines shows the upper and lower contacts of the Unit IV massive oxide gabbro.

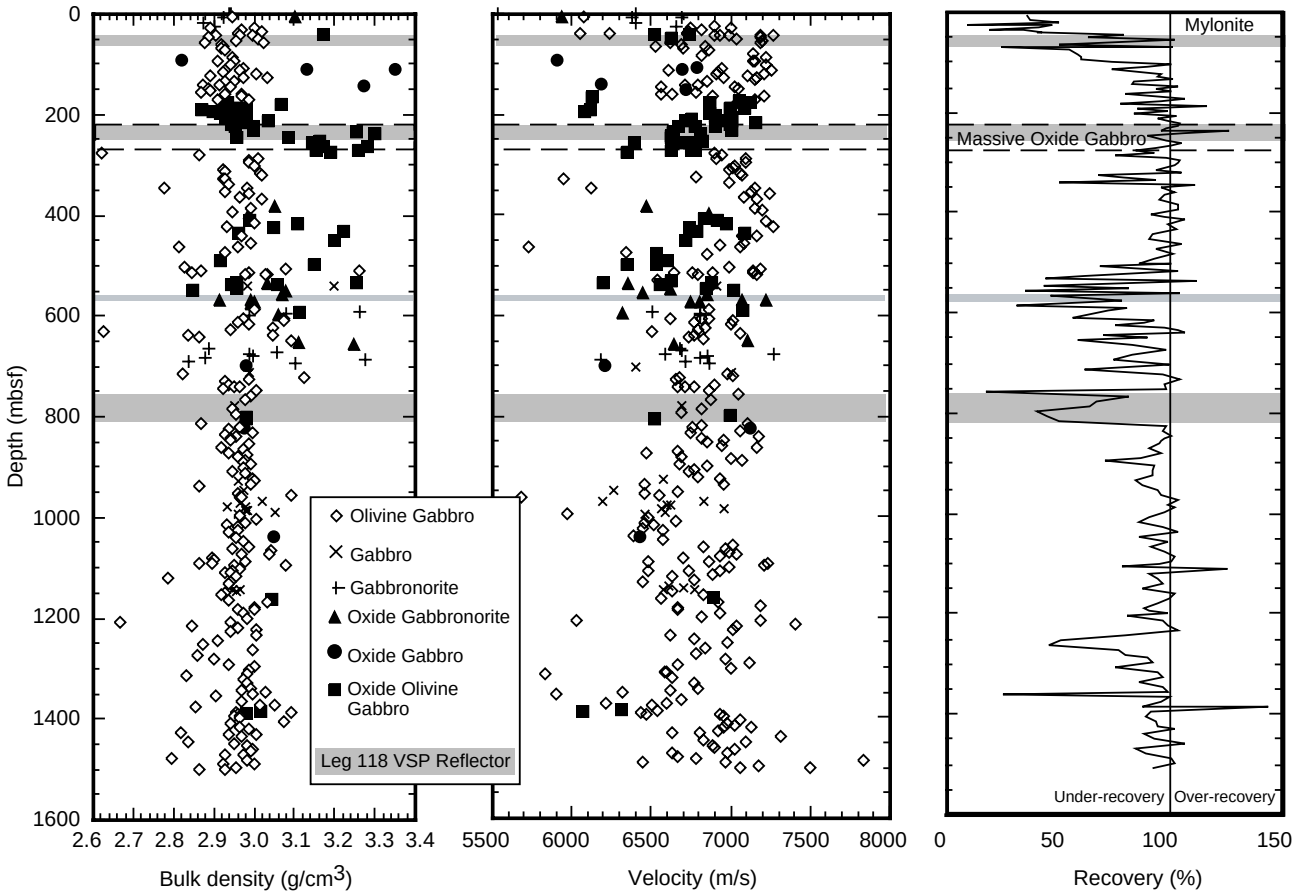

Table T1. Averaged chemical compositions of samples from Hole 735B as a function of rock type and depth in the drill core.

Rock type	Depth interval (mbsf)	*N*	SiO_2 (wt%)	TiO_2 (wt%)	Al_2O_3 (wt%)	Fe_2O_{3T} (wt%)	MnO (wt%)	MgO (wt%)	CaO (wt%)	Na_2O (wt%)	K_2O (wt%)	P_2O_5 (wt%)	$\%Fe^{2+}$	Mg#	Ca#	V (ppm)	Cr (ppm)	Ni (ppm)	Cu (ppm)	Zn (ppm)	Rb (ppm)	Sr (ppm)	Y (ppm)	Zr (ppm)	Nb (ppm)
Felsic	(*)	3	64.06	1.62	18.49	1.80	0.05	1.27	4.93	6.24	1.43	0.11	76	0.60	0.26	41	0	12	13	8	9	133	68	184	19
Oxide gabbro	520-705	5	46.55	2.97	12.24	17.69	0.27	6.06	9.99	3.27	0.10	0.86	67	0.51	0.63	311	6	34	68	131	2	159	63	74	4
	800-960	6	47.33	2.84	12.80	14.81	0.22	7.36	11.20	2.86	0.06	0.53	77	0.57	0.69	558	140	98	105	101	<1	141	47	81	2
	960-1320	2	48.30	2.31	15.01	13.38	0.21	6.13	10.06	3.40	0.08	1.12	74	0.55	0.62	274	59	69	96	121	1	193	63	84	6
Gabbro	520-705	4	52.21	0.52	16.72	7.40	0.13	7.38	12.13	3.43	0.06	0.02	79	0.72	0.66	196	13	63	36	44	1	193	15	43	1
	705-800	2	51.24	0.47	16.37	6.78	0.13	9.03	13.16	2.76	0.03	0.02	89	0.75	0.72	183	198	105	92	44	<1	163	12	33	<1
	800-960	7	51.04	0.43	16.38	6.93	0.14	8.97	13.21	2.84	0.03	0.03	86	0.75	0.72	175	145	86	86	42	1	167	13	36	1
	960-1320	6	51.75	0.38	16.37	6.45	0.13	8.77	13.15	2.97	0.03	0.01	89	0.75	0.71	179	65	77	75	39	1	176	12	25	1
	1320-1503	7	51.55	0.35	17.94	5.16	0.11	8.37	13.52	2.95	0.03	0.01	83	0.79	0.72	152	130	86	70	28	1	187	11	28	<1
Olivine gabbro	520-705	12	51.50	0.44	16.18	7.78	0.14	8.85	11.91	3.13	0.06	0.02	91	0.71	0.68	178	49	78	68	48	<1	172	13	50	2
	705-800	11	50.65	0.34	16.46	6.93	0.13	10.16	12.67	2.63	0.02	0.02	90	0.76	0.73	159	179	131	99	43	<1	163	9	26	1
	800-960	22	50.74	0.44	15.91	7.10	0.13	10.23	12.71	2.69	0.03	0.03	90	0.75	0.72	163	216	118	70	46	<1	161	12	36	<1
	960-1320	40	51.04	0.42	16.37	7.16	0.13	9.41	12.56	2.85	0.03	0.02	88	0.75	0.71	164	93	96	79	44	1	171	10	34	1
	1320-1503	18	51.14	0.36	16.99	5.80	0.12	9.29	13.62	2.65	0.02	0.02	88	0.78	0.74	174	171	103	67	35	1	168	11	26	1
Troctolitic gabbro	800-960	2	50.95	0.36	17.29	6.19	0.12	9.26	13.05	2.68	0.08	0.02	93	0.76	0.73	167	256	105	55	38	3	161	12	33	1
	1320-1503	3	49.29	0.28	17.90	7.84	0.13	10.70	11.11	2.72	0.02	0.01	87	0.76	0.69	104	188	174	74	47	<1	180	10	25	<1
Troctolite	500-520	4	46.99	0.13	18.21	6.52	0.10	15.52	10.65	1.81	0.06	0.01	95	0.83	0.77	58	606	452	74	43	2	149	6	20	1

Notes: Depth interval cutoffs correspond to the chemical stratigraphy units (see **"Geochemistry,"** p. 16). *N* = number of samples used to calculate the average. (*) = average of three felsic samples with less than 3% Fe_2O_3; the mixed felsic/mafic rock samples have been excluded. $\%Fe^{2+}$ = percentage of total iron present as ferrous iron; Mg# = $(Mg/Mg+Fe^{2+})$ molar, calculated from $\%Fe^{2+}$. Ca# = (Ca/Ca+Na)molar. Concentration units = weight percent for the major element oxides; parts per million for the minor and trace elements. Major element compositions are all normalized to sum = 100%.